

A zero-dimensional model for high-energy scattering in QCD

J.-P. Blaizot ^{a,1,2}, E. Iancu ^{b,1,2}, and D.N. Triantafyllopoulos ^{a,1}

^a *ECT , Villa Tambosi, Strada delle Tabarelle 286, I-38050 Villazzano (TN), Italy*

^b *Service de Physique Theorique, CEA Saclay, CEA/DSM/SPHT, F-91191 Gif-sur-Yvette, France*

Abstract

We investigate a zero-dimensional toy model originally introduced by Mueller and Salam [1] which mimics high-energy scattering in QCD in the presence of both gluon saturation and gluon number fluctuations, and hence of Pomeron loops. Unlike other toy models of the reaction-diffusion type, the model studied in this paper is consistent with boost invariance and, related to that, it exhibits the same mechanism for particle saturation as the JIMWLK equation in QCD, namely the saturation of the emission rate due to high-density effects. Within this model, we establish the dominant high-energy behaviour of the S -matrix element $\langle S^n \rangle$ for the scattering between a generic target and a projectile made with n particles. Remarkably, we find that all such matrix elements approach the black disk limit $S = 0$ at high rapidity Y , with the same exponential law: $\langle S^n \rangle \sim \exp(-Y)$ for all values of n . This is so because, in the vicinity of the unitarity limit, the S -matrix is dominated by rare target configurations which involve only few particles. We also find that the bulk distribution deeply at saturation is of the Poisson type.

¹ *E-mail addresses:* blaizot@ect.it (J.-P. Blaizot), iancu@ds-mail.cea.fr (E. Iancu), dionysis@ect.it (D.N. Triantafyllopoulos).

² Membre du Centre National de la Recherche Scientifique (CNRS), France.

1 Introduction

Much of the recent progress in the field of high-energy QCD has come from the gradual understanding [2–26] of the analogies between the gluon evolution in QCD at high energy and a classical stochastic process, similar to the ‘reaction–diffusion process’ $A \rightarrow AA$ [27, 28]. Such analogies lead to the conclusion that the properties of the QCD scattering amplitudes at very high energy, including in the vicinity of the unitarity limit, are strongly influenced by *gluon–number fluctuations* in the dilute regime, and hence cannot be reliably computed from mean field approximations like the Balitsky–Kovchegov (BK) equation [5, 6]. Although at a first sight surprising — since the high-energy regime is characterized by high gluon occupancy, and therefore should be less affected by fluctuations —, such a strong sensitivity to fluctuations was in fact noticed in early studies of unitarization in the context of the dipole picture [2–4] and, more recently, it has been rediscovered within the context of the non-linear QCD evolution in the vicinity of the saturation line [12, 14].

It has been realized [17] that the relevant fluctuations are missed by the JIMWLK equation [7–9], which describes the non-linear evolution of the gluon distribution in the (high-density) target, as well as by its ‘dual’ counterpart, the Balitsky hierarchy [5] for the scattering amplitudes, in which the evolution is rather encoded in the wavefunction of the (dilute) projectile. The JIMWLK equation properly encompasses the mechanism responsible for gluon saturation at high density, but it misses the correlations associated with gluon splitting in the dilute regime. Correspondingly, the Balitsky equations faithfully describe the splitting processes within the projectile, but completely ignore the non-linear effects responsible for saturation.

At the same time, new equations have been proposed [17–20], which heuristically combine the dipole picture in the dilute regime with the JIMWLK evolution at high density, thus leading to a generalization of the Balitsky hierarchy which encompasses both saturation and fluctuation effects in the limit where the number of colors N_c is large, $N_c \rightarrow \infty$. These equations have been interpreted [23] as an effective theory for BFKL ‘pomeron’, in which the pomerons are allowed to dissociate and recombine with each other, like the ‘molecules’ in the reaction–diffusion problem. (See also Ref. [29] for a related approach in the context of nucleus–nucleus scattering.) But the complexity of these ‘Pomeron loop’ equations has so far hindered any systematic approach towards their solutions, including via numerical methods. The only properties of these solutions to be presently known come essentially from the correspondence with statistical physics [13–15, 17, 30, 31], which is however limited to asymptotically high energies and very small values of the coupling constant.

In view of the complexity of the QCD of the problem, several authors [17, 32–35] have recently started investigating simpler, zero-dimensional, models that allow for analytic studies of the approach towards saturation and unitarization with increasing energy. The models discussed in Refs. [17, 32, 34, 35] are all borrowed from statistical physics and describe a $A \rightarrow AA$ reaction process. The model briefly discussed in Ref. [33] has been originally proposed by Mueller and Salam [1] as a toy model for ‘dipole’ evolution in the presence of saturation, and seems to be the closest to the actual QCD dynamics, as we shall explain at length in what follows. This is the model that we shall focus on in this paper.

At this point, one may legitimately wonder about the usefulness of *any* zero-dimensional model in the context of the high-energy evolution in QCD. As well known, this evolution is genuinely non-local in transverse momentum, and this non-locality is responsible for the main

characteristic of a hadron wavefunction at sufficiently high energy, namely, the coexistence of two different phases at different values of the gluon transverse momentum k_\perp : (i) a dilute phase at large k_\perp , where the standard, linear (or ‘leading-twist’), perturbative evolution applies and (ii) a high-density phase, also known as the *color glass condensate* [9, 36, 37], at relatively low k_\perp , where the dynamics is fully non-linear and the gluon occupation factor (almost) saturates. With increasing energy, the CGC phase extends towards larger values of k_\perp , and the main physical questions refer to the rate of this expansion and to the properties of the gluon distribution and of the scattering amplitudes in the vicinity of the *saturation line* — i.e., in the transition region from dense to dilute [38–40]. In particular, it is precisely in this region that the effects of the gluon-number fluctuations are most striking [14, 15, 17]: they considerably slow down the energy increase of the saturation momentum and render the saturation line diffuse, which in turn has important consequences for the measured cross-sections [41, 42].

Clearly, all these interesting features will be lost once one restricts oneself to a fully local, zero-dimensional, problem. But even in that limit, some non-trivial questions remain, whose detailed understanding could shed light on the physics of saturation in the presence of particle-number fluctuations. Chiefly among these, there is the problem of the approach of the (average) S -matrix element $\langle S \rangle$ towards the black disk limit $\langle S \rangle = 0$ with increasing energy. The arguments presented in Refs. [1, 12] as well as the analysis to be presented in this paper suggest that this approach is strongly influenced by the fluctuations: the average S -matrix near the unitarity limit is dominated by *atypical* configurations, which have a relatively low gluon occupancy — well below the average occupancy at that energy — and thus yield a large contribution $S \rightarrow 1$ to the average quantity $\langle S \rangle$. The qualitative arguments in Refs. [1, 12] have been confirmed by most previous studies of zero-dimensional models [1, 4, 32, 34], yet some disagreement persists in the literature [35]. Actually, the results in Ref. [35] dispute even the fact that the black disk limit should be eventually approached at sufficiently high energy: they rather advocate a ‘gray disk’ limit. These results will be critically discussed in this paper (see Appendix B).

The effect of fluctuations that we have just discussed has an interesting implication for the S -matrix $\langle S^n \rangle$ of a projectile made with n particles, which to our knowledge has not been previously noticed in the literature. As well known, the quantity $\langle S^n \rangle$ measures the probability that the system of n particles emerge unscattered. Simple arguments of the mean-field type suggest that $\langle S^n \rangle \rightarrow \langle S \rangle^n$ at high energy. (For instance, this is the prediction of the Balitsky–JIMWLK equations.) However, if the average S -matrix is dominated by *rare* configurations for which $S \rightarrow 1$ per incoming particle, then for these relevant configurations we have $S^n \rightarrow S \rightarrow 1$ for any n , which after averaging yields $\langle S^n \rangle \rightarrow \langle S \rangle$, in sharp contrast with the mean field expectation. As we shall demonstrate here, this prediction that $\langle S^n \rangle \rightarrow \langle S \rangle$ is indeed verified within the zero-dimensional model that we shall investigate.

Let us now explain why, in our opinion, the model introduced by Mueller and Salam in Ref. [1] is indeed closer to the actual QCD dynamics than the (zero-dimensional) reaction model $A \rightarrow A A$ (although the latter appears to more widely studied in the recent literature). The main reason is that the Mueller–Salam model correctly captures the QCD mechanism for the saturation of the particle number at high energy, which is *not* particle recombination (as in the reaction–diffusion process), but rather the *saturation of the rate for particle emission due to high-density effects*. The new particle which is emitted when increasing the rapidity in one step can be radiated off any of the particles created in the previous steps and, moreover, it can undergo multiple scattering off the latter. When the density is relatively low (the low–

energy case), the emission rate is simply proportional to the total number of sources, leading to an exponential increase of the number of particles with the rapidity Y . But when the density becomes large enough for multiple scattering to be important, the emission rate saturates at a constant value, independent of the number of particles in the system. Then, the number of particles keeps growing, but only *linearly* in Y . This ‘almost saturation’ scenario is indeed similar to the physical mechanism at work in QCD [43,44], where gluon saturation — as described by the JIMWLK equation — proceeds precisely via the saturation of the rate for gluon emission by strong color field effects (see also the discussion in Refs. [10,45,46]). By contrast, in the reaction–diffusion process, the particle (occupation) number saturates at a *fixed* value (independent of Y), a situation which looks unphysical from the perspective of QCD: when increasing the rapidity even within the saturation domain, the gluon phase–space opens towards lower longitudinal momenta, which then allows for further radiation.

Closely related to the above, there is a second reason why the Mueller–Salam model is better suited to mimic the QCD evolution than the reaction model : unlike the latter, the former is consistent with the *boost invariance* of the S –matrix in the presence of multiple scattering. In fact, in Ref. [1], this model has been constructed precisely by imposing boost invariance — i.e., by requiring the (average) S –matrix to be independent upon the choice of a Lorentz frame — on the scattering between two systems of particles which evolve in the same way with increasing rapidity. Remarkably, within this zero–dimensional context, the requirement of boost invariance together with the assumption of one particle emission per unit rapidity are in fact sufficient to fix uniquely the rate at which a system of n particles can emit another one, and predict, in particular, the saturation of this rate for sufficiently large values of n . If, on the other hand, the target and projectile are assumed to evolve according to a reaction model ($A \rightarrow AA$) including particle splitting ($A \rightarrow AA$) and particle recombination ($AA \rightarrow A$), then one can easily check that the boost invariance is broken by the recombination process, within a factorization scheme which allows for the multiple scattering of the individual particles (see Appendix A).

Recently, the requirement of boost invariant has been shown to imply a rather strong constraint (or symmetry property) on the structure of the evolution equations, known as the *self–duality* of the evolution Hamiltonian [22,23]. As noticed in Ref. [33], the MS model obeys indeed this self–duality property (as it should, given that it generates a boost–invariant evolution). In this respect, the structure of the MS model bears some resemblance to the self–dual ‘diamond’ Hamiltonian proposed within the context of QCD in Refs. [24,25]. On the other hand, the evolution associated with the reaction–diffusion process is *not* self–dual.

Our subsequent analysis will reveal some other interesting results, that one may expect to have a counterpart in QCD as well. For instance, we shall find a pronounced difference between the case where the projectile consists in a single particle and that where it involves two or more such particles: While for $n \geq 2$, the average S –matrix element $\langle S^n \rangle$ is fully controlled (in the high–energy regime of interest) by the rare target configurations which are dilute, and thus is insensitive to the physics of saturation, on the other hand, for $n = 1$, we shall find that $\langle S \rangle$ is still sensitive, although marginally, to quasi–saturated target configurations with high occupation numbers. (Our result for $\langle S \rangle$ will be the same as in the original analysis in Ref. [1], where however the precise nature of the relevant configurations has not been investigated.) In turn, this leads to a significant difference between these two cases — $n = 1$ and $n \geq 2$ — in so far as the *subleading* behaviour at high energy is concerned (the leading, exponential, behaviour being the same in both cases).

We also investigate the nature of the particle distribution in a single wavefunction (say, that of the target) at high energy. We shall thus distinguish between the tail of the distribution at low occupation numbers — this describes the dilute configurations which control the average S -matrix — and the bulk of the distribution at high occupation numbers, which describes the typical, saturated, configurations and is found to be Poissonian.

In addition to such explicit results concerning the high-energy behaviour of the average S -matrix or of the particle distribution, the formal structure of the model (in particular, the associated evolution equations) is interesting as well, as it might be inspiring in view of further studies in QCD.

The paper is structured as follows: In Sect. 2, we shall first construct the master equation for the toy model, from the requirement of boost invariance, and then exploit this equation in order to derive evolution equations for the observables, like the S -matrix element $\langle S^n \rangle$ for a projectile made with n particles. In Sect. 3 we shall use the solution to the master equation (whose Laplace transform is known exactly) in order to deduce the high-energy behaviour of the S -matrix elements $\langle S^n \rangle$ with $n \geq 1$ (in Sect. 3.1) and of the bulk of the particle distribution (in Sect. 3.2). Finally, in Sect. 4, we shall discuss the correspondence between the toy model and the high-energy problem in QCD, with emphasis on the similarity between the respective evolution equations in various limits. Some other issues — like the lack of boost invariance for the recombination process, or the relation with the reaction toy model of Ref. [35] — are left for Appendices.

2 The toy model: Structural aspects

As explained in the Introduction, the toy model that we shall consider is ‘zero-dimensional’ in the sense that its only variable is the rapidity interval Y which controls the high-energy evolution. The ‘physical’ problem that we have in mind is that of the scattering between two systems of particles, referred to as the projectile and the target. Each system is characterized by a probability distribution giving the number of particles it contains at a given rapidity. During the collision of the two systems, particles of the projectile and the target undergo independent collisions, characterized by a scattering amplitude σ . In order to keep close contact with QCD, we shall use throughout a QCD-inspired terminology and refer to the two colliding systems as two “onia” and to the particles which compose these onia as “dipoles”. This is suggestive since, in the dilute regime at least, the evolution that we shall describe corresponds to the zero-dimensional version of Mueller’s dipole picture [1–4].

The number of particles in each system depends upon its rapidity, and therefore on the frame. We put the right mover (the ‘target’) at rapidity $Y = Y_0$ and the left mover (the ‘projectile’) at rapidity $Y = Y_0$ ($Y_0 > 0$). We denote by $P_m^L(Y_0)$ the probability to find exactly m dipoles inside the projectile at rapidity Y_0 . Similarly $P_n^R(Y_0)$ will be the corresponding distribution for the target. Allowing the dipoles in each onia to scatter independently with each other, the S -matrix for a configuration with m dipoles in the projectile and n dipoles in the target takes the factorized form $S = \langle S^{m,n} \rangle$, where $\langle S \rangle = 1$ is the S -matrix for the scattering between two elementary dipoles and σ is the corresponding T -matrix. The most interesting case in view of the comparison with QCD is the weak coupling regime $\sigma \ll 1$ (see Sect. 4).

The physical S -matrix is obtained by averaging over all the possible configurations in the

two onia, with the respective probability distributions:

$$\langle S \rangle_Y = \sum_{m, n=1}^X P_m^L(Y_0) P_n^R(Y - Y_0)^{m, n}; \quad (2.1)$$

This expression for the S-matrix reflects the fundamental factorization assumption which lies at the basis of our analysis. This formula was used in Ref. [33], while in their original formulation, Mueller and Salam [1] write, in their analog of Eq. (2.1), $e^{-m, n}$ in place of $P_m^L P_n^R$.

2.1 Particle saturation from boost invariance

We shall assume that the two onia follow the same evolution law in rapidity, and obey the same initial condition at $Y = 0$, so that $P_n^R(Y) = P_n^L(Y)$. For definiteness, we shall assume that each of them consists of only one dipole at $Y = 0$, i.e., $P_n^R(0) = P_n^L(0) = \delta_{n,1}$. Then, as we show now, the rapidity evolution is uniquely fixed by the following two constraints:

- (i) Lorentz (boost) invariance: The total S-matrix should be independent of the choice of frame, i.e., of Y_0 , which implies

$$\frac{d \langle S \rangle}{dY_0} = 0; \quad (2.2)$$

- (ii) The onium evolves through dipole emission, in such a way that only one new dipole can be produced under a step dY in rapidity. Thus, in a step dY , a system of n dipoles can turn into a system of $n + 1$ dipoles, with a probability $f_n dY$, and stay in its initial configuration with a probability $1 - f_n dY$. It follows that the probability $P_n(Y)$ evolves according to the following master equation:

$$\frac{dP_n(Y)}{dY} = f_{n-1} P_{n-1}(Y) - f_n P_n(Y); \quad (2.3)$$

where f_n is a function of n to be determined shortly. In this equation and throughout, P_n refers generically to either P_n^R , or P_n^L . Note that the evolution (2.3) preserves the total probability: $d(\sum_n P_n(Y)) = dY = 0$.

As noticed in Ref. [1], the two conditions above determine the transition probabilities f_n up to an overall normalization factor (which is then fixed by f_1). Indeed, setting the derivative of Eq. (2.1) with respect to Y_0 equal to zero and using Eq. (2.3) we arrive at

$$\sum_{m, n=1}^X P_m^L(Y_0) P_n^R(Y - Y_0)^{m, n} [f_m (1 - f_n) - f_n (1 - f_m)] = 0 \Rightarrow f_n = c (1 - f_n); \quad (2.4)$$

where c is a constant and can be reexpressed as $c = f_1/(1 - f_1)$, where f_1 is the rate of splitting of one dipole into two. Without loss of generality, we shall set $f_1 = 1$. (Within the QCD dipole picture, this rate would be equal to $\alpha_s/2$ times the dipole kernel; see, e.g., Refs. [2, 11] for details.) We then obtain, from Eq. (2.4),

$$f_n = \frac{1 - f_n}{1 - f_1} = 1 + \frac{f_n - 1}{1 - f_1} \Rightarrow f_n = 1; \quad (2.5)$$

The quantity f_n is the rate at which a system of n dipoles emits an extra one in a step dY in rapidity. The constraint of boost-invariance of the scattering matrix forces the f_n (and hence the probability distribution P_n) to depend on Y , and furthermore induces non trivial correlations that affect their n -dependence. To better visualize the implications of Eq. (2.5), it is useful to consider the two limits of strong ($\alpha \gg 1$) and weak ($\alpha \ll 1$) couplings. In the weak coupling regime, $\alpha \ll 1$ and $f_n \propto n$: in this regime, the n dipoles split independently of each other. In the strong coupling regime however, $\alpha \gg 1$, and $f_n \propto 1$: in this case correlations in the n -dipole system are such that only a single dipole can be emitted.

But even when α is fixed and small, which is the case of physical interest, a similar change of regime occurs when increasing the value n . Namely, Eq. (2.5) implies that, when $\alpha \ll 1$, the rate f_n has the following limiting behaviors:

$$\frac{f_n}{n} \approx \begin{cases} 1 - \frac{(n-1)}{2} & \text{for } n \ll 1/\alpha \\ \frac{1}{n} & \text{for } n \gg 1/\alpha \end{cases} \quad (2.6)$$

According to Eq. (2.6), the emission rate f_n saturates at a large, but constant, value $1/\alpha$ when $n > n_{\text{sat}} = 1/\alpha$. As we shall discover soon, this is indeed the order of magnitude of the average dipole number at the onset of saturation.

Alternatively, observing that S^n is the S -matrix for the scattering of a dipole projectile on an n -dipole target, we may interpret the presence of higher powers of α in the emission rate (2.5) as reflecting the *multiple scattering* between the newly emitted dipole and its sources. This interpretation becomes perhaps more transparent when Eqs. (2.3) and (2.5) are used to compute the rate for the evolution of the average S -matrix with Y . One finds

$$\frac{d \langle S \rangle}{dY} = - \frac{1}{2} \sum_{m,n} P_m^L(Y_0) P_n^R(Y - Y_0) t_m^n (1 - t_m) (1 - t_n); \quad (2.7)$$

where the quantities $t_n = 1 - \alpha^n$ and $t_m = 1 - \alpha^m$ can be recognized as the scattering amplitudes for the scattering between one dipole — the one created in the last step in the evolution — and the n preexisting dipoles in the target and, respectively, the m dipoles in the projectile.

For latter reference, let us notice that Eq. (2.1) is equivalent to the following factorized form of the *scattering amplitude* $\langle H \rangle = 1 - \langle S \rangle$

$$\langle H \rangle_Y = \sum_{k=1}^{\infty} \frac{(\alpha)^{k-1}}{k!} h_n^{(k)} i_{Y_0} h^k i_{Y - Y_0}; \quad (2.8)$$

which is the form generally used in the QCD context (see, e.g., Refs. [6,16,26]). In this equation, $h_n^{(k)} i = h_n(n-1) \dots (n-k+1) i$ is the k -body normal-ordered dipole density (here, in the wavefunction of the projectile), $t = 1 - \alpha$ is the scattering amplitude for a single dipole, and $h^k i_{Y - Y_0}$ is the average amplitude for the simultaneous scattering of k dipoles off the target.

Finally, let us mention that the P_n 's can be obtained from the following generating functional

$$Z(u; Y) = \sum_{n=1}^{\infty} P_n(Y) u^n; \quad (2.9)$$

from which most quantities of interest can also be derived. In particular, the S -matrix for the scattering of a projectile made with m dipoles is

$$hS^m_i = Z(u = \frac{m}{Y}; Y): \quad (2.10)$$

Differentiating Eq. (2.9) with respect to Y and using the master equation one arrives at

$$\frac{dZ}{dY} = \frac{1}{Y} [Z(u) - Z(u + \frac{1}{Y})]: \quad (2.11)$$

This equation turns out to be difficult to solve analytically, so in what follows we shall work mostly with the master equation. But Eq. (2.11) will be used in Appendix B in order to make contact with the analysis of the reaction $(A \rightarrow A A)$ toy model in Ref. [35].

2.2 Evolution equations: Saturation, unitarity & fluctuations

Using the master equation (2.3), we shall now deduce evolution equations for physical quantities such as the average S -matrix or the average dipole density, and study some of their general properties. More specific predictions about the solutions to these equations at high energy will be discussed in Sect. 3.

Let us begin with the scattering problem and rewrite Eq. (2.1) as

$$hS^m_i = \sum_m P_m^L(Y_0) hS^m_{i_Y - Y_0} \quad (2.12)$$

where

$$hS^m_i = \sum_n P_n^R(Y) hS^{m+n}_i \quad (2.13)$$

is the average S -matrix for a projectile made with m dipoles and a generic target. It is therefore interesting to study the case where the number of dipoles m within the projectile is fixed.

From Eqs. (2.13), (2.3) and (2.5), it is now straightforward to obtain the following evolution equation for hS^m_i :

$$\frac{d hS^m_i}{dY} = f_m hS^{m+1}_i - hS^m_i: \quad (2.14)$$

This is not a closed equation — hS^m_i being related to hS^{m+1}_i —, but rather a particular equation from an infinite hierarchy. This equation has been obtained here by following the evolution of the target (namely, by using Eq. (2.3) for P_n^R), but it can be easily reinterpreted as describing evolution in the projectile: when increasing the projectile rapidity by dY , the incoming system of m dipoles can turn, with a rate f_m into a system of $(m + 1)$ dipoles, which then scatters off the target with an S -matrix hS^{m+1}_i . This is the origin of the first term within the brackets in the r.h.s. of Eq. (2.14). As for the second term, involving $(-hS^m_i)$, it corresponds to the case where the system remains intact during the evolution (which occurs with probability $1 - f_m dY$).

For $m = 1$ (a single dipole in the projectile), Eq. (2.14) reduces to

$$\frac{d hS_i}{dY} = hS^2_i - hS_i; \quad (2.15)$$

which is formally identical to the first equation in the Balitsky–JIMWLK hierarchy. However, differences with respect to the latter appear already for $m = 2$. Indeed we have

$$\frac{d h s^2 i}{dY} = (2 - \frac{h}{m}) h s^3 i - h s^2 i ; \quad (2.16)$$

The corresponding Balitsky equation³ would involve a factor 2 in place of $(2 - \frac{h}{m})$ in the r.h.s. More generally the Balitsky equations are obtained by replacing \mathbb{E}_m by m in the r.h.s. of Eq. (2.14), which amounts to ignoring *saturation* effects in the *projectile*. Such effects may be expected to be negligible when $m \rightarrow \infty$, but we shall discover in the next section that this is not so. In fact they are essential to get the correct description of the evolution at large Y .

Alternatively, the difference between the hierarchy in Eq. (2.14) and the corresponding Balitsky hierarchy can be attributed to *particle–number fluctuations* in the *target*. To see that, observe that for $n \rightarrow \infty$ the discrete nature of n is inessential, and the associated fluctuations become relatively unimportant. For large n , we can then treat n as a continuum variable and replace the finite difference in the r.h.s. of Eq. (2.3) by a derivative w.r.t. n :

$$\frac{d P_n(Y)}{dY} = - \frac{1}{n} \frac{\partial}{\partial n} (1 - \frac{h}{n}) P_n(Y) \quad \text{when } n \rightarrow \infty : \quad (2.17)$$

At the same time, we can trade the sum over n in the definition (2.13) of the average S –matrix $h s^m i$ by the corresponding integral. Then, it is easily to check that Eq. (2.17) implies again⁴

$$\frac{d h s^m i}{dY} = - \frac{h}{m} h s^{m+1} i - h s^m i ; \quad (2.18)$$

where we have also used $j n \rightarrow n$, as appropriate for $n \rightarrow \infty$.

The fact that neglecting the correlations associated with particle–number fluctuations in the target is equivalent to ignoring the saturation effects in the projectile is in agreement with the general arguments in Ref. [17]. Further insight on this issue can be gained by rewriting the evolution equations in terms of the scattering amplitudes $h t^k i$ introduced in Eq. (2.8). The corresponding equations are easily deduced from those for $h s^m i$ by using $t = 1 - s$. The first three equations in this hierarchy read:

$$\frac{d h t i}{dY} = h t i - h t^2 i ; \quad (2.19)$$

$$\frac{d h t^2 i}{dY} = 2 h t^2 i - 2 h t^3 i + h t (1 - t^2) i ; \quad (2.20)$$

$$\frac{d h t^3 i}{dY} = 3 h t^3 i - 3 h t^4 i + 3 h t^2 (1 - t^2) i + 2 h t (1 - t^3) i ; \quad (2.21)$$

The new terms, as compared to the corresponding Balitsky equations, are those proportional to t or t^2 in the last two equations. As mentioned before, these terms reflect dipole–number fluctuations in the target. Let us first consider Eq. (2.20): Among the three fluctuation terms

³ In the remaining part of this section, by the “Balitsky equations” we shall mean the simplified version of these equations at large- N_c and for zero transverse dimensions, that is, Eq. (2.14) with $\mathbb{E}_m \rightarrow m$.

⁴ In Sect. 4, we shall argue that Eq. (2.17) is the toy–model analog of the JIMWLK equation.

there, namely $h_{t|1}^{(t)} = h_{t|2}^2 + t_{t|1}$, we shall focus on the last one, $h_{t|1}$, since this is the most important one⁵. (When $t_{t|1} \ll 1$, the other terms are negligible in all regimes.) Although formally suppressed by a power of $t_{t|1}$ with respect to the (BFKL-like) term $h_{t|2}^2$, the fluctuation term $h_{t|1}$ is in fact equally important in the low density regime where $h_{t|1} \ll 1$. To clarify its physical meaning, note that, in the dilute regime, the average dipole scattering amplitude is simply proportional to the average particle number in the target: $h_{t|1} \propto n_{t|1}$. Thus, $h_{t|1} \propto n_{t|1}$, and the physical interpretation becomes transparent: under a rapidity step dY , any one among the $n_{t|1}$ target dipoles can split into two and then the child dipoles can scatter with the two projectile ones, with strength $t_{t|1}^2$. Thus, the simultaneous scattering of two projectile dipoles gives us access to the correlations induced via dipole splitting in the target.

Let us now move to the higher equations in the hierarchy. Eq. (2.21) for $h_{t|3}$ contains two *relevant* fluctuation terms, of order $h_{t|2}^2$ and $t_{t|1}^2 h_{t|1}$, respectively. The first one has the same physical origin as the term $h_{t|1}$ in the equation for $h_{t|2}$: that is, two among the three projectile dipole ‘feel’ a fluctuation by scattering off the child dipoles produced by a splitting in the target. The second term, $t_{t|1}^2 h_{t|1} \propto n_{t|1}^3$, describes the process in which the fluctuation is felt by all the three projectile dipoles: e.g., two of them scatter off one child dipole, and the third one scatters off the other child dipole. These terms are both relevant since they are of the same order in the low density region where $h_{t|1} \ll 1$. It is not hard to understand the generalization to higher equations in this hierarchy: the equation for $h_{t|k}$ will involve relevant fluctuation terms of the following types: $h_{t|k-1}^2, t_{t|1}^2 h_{t|k-2}, \dots, t_{t|1}^{k-1} h_{t|1}$. All such terms are important for building up many-body correlations in the dilute regime.

Eq. (2.19) allows us to estimate the rapidity Y_c for the onset of unitarity corrections in the dipole–target scattering. Indeed, at $Y = 0$, $h_{t|k}^{(0)} = t_{t|k}^k$, hence $h_{t|k+1}^{(0)} \ll h_{t|k}^{(0)}$ and these inequalities will be preserved in the early stages of the evolution where one can therefore neglect $h_{t|2}^2$ as compared to $h_{t|1}$ in the r.h.s. of Eq. (2.19). This then leads to $h_{t|1} \propto e^Y$, the analog of the BFKL increase [47]. Clearly this ceases to be correct when $h_{t|1} \sim 1$, that is, for $Y \sim Y_c \equiv \ln(1/t_{t|1})$. For larger rapidities $Y > Y_c$, multiple scattering becomes important and ensures the unitarization of the dipole amplitude ($h_{t|1} \rightarrow 1$ as $Y \rightarrow \infty$), as we shall discover in the next section.

Equivalently, Y_c marks the onset of the saturation effects in the target in the frame in which the projectile is dilute. To see this, consider the evolution equation for the average particle number $n_{t|1}$ in the target, that is

$$\frac{dn_{t|1}}{dY} = \frac{1}{h_{t|1}} h_{t|1}^2 n_{t|1}; \quad (2.22)$$

where $h_{t|1}^2 n_{t|1} = h_{t|1}$ is recognized⁶ as the scattering amplitude for a projectile made with one dipole, cf. Eq. (2.13). At low density, $h_{t|1}^2 n_{t|1} \propto n_{t|1}$, and the particle number exhibits the exponential growth $n_{t|1} = e^Y$ characteristic of BFKL evolution. But when $n_{t|1}$ becomes as large as $n_{\text{sat}} \equiv 1/t_{t|1}$, which happens for $Y \sim Y_c$ the growth is tamed by non-linear effects. Eventually, when $Y \gg Y_c$, $h_{t|1}^2 n_{t|1}$ becomes negligible so that $dn_{t|1}/dY \rightarrow 0$ and $n_{t|1}$ grows only linearly (as expected for the gluon occupation factor in QCD [43, 44]). To summarize,

⁵ This is the analog of the ‘fluctuation terms’ which appear in the Pomeron loop equations constructed in Refs. [17, 18]. See the discussion in Sect. 4.

⁶ Alternatively, the r.h.s. of Eq. (2.23) is recognized as the average emission rate $h_{t|1}^2 n_{t|1}$.

$$h n i = e^Y \quad \text{when} \quad Y < Y_c; \quad h n i \sim \frac{Y}{Y_c} \quad \text{when} \quad Y > Y_c: \quad (2.23)$$

3 The high-energy behaviour of the toy model

In this section, we shall establish the dominant high-energy (i.e., large- Y) behaviour predicted by the toy model for the dipolar S -matrix elements $h s^m i$ with $m \geq 1$, and also for the particle distribution in the target.

3.1 The dipole S -matrix elements $h s^m i$

The dominant high-energy behaviour of the dipole S -matrix elements $h s^m i_Y$ will be obtained by solving the master equation, Eq. (2.3), with the initial condition $P_n^R(0) = \delta_{n1}$ and then performing the sum over n in Eq. (2.13) (in the approximations of interest).

But before we do that, we note that the hierarchy in Eq. (2.14) admits the following, two-parameter, family of solutions:

$$h s i_{as} = \frac{A}{1} (Y - Y_0) e^{-Y} \quad \text{and} \quad h s^m i_{as} = \frac{A}{1} \frac{m-2}{m-1} e^{-Y} \quad \text{for} \quad m \geq 2; \quad (3.1)$$

with arbitrary values for the parameters A and Y_0 . Although these cannot be the complete solutions, as they do not obey the physical initial conditions at $Y = 0$ for any choice of the free parameters, with the choices $A = 2$ and $Y_0 = Y_c - \ln(1/2)$ they describe the *asymptotic* form of the physical solutions at large $Y > Y_c$ (hence the subscript 'as'), as we shall see.

What is remarkable about the behaviour of these solutions is the fact that, for asymptotically large Y , all the $h s^m i_Y$'s approach the black disk limit ($S = 0$) according to the *same* exponential law $\exp(-Y)$, for all m . This might look counterintuitive since, at large Y , the target onium is typically characterized by a large number of dipoles, off which a projectile dipole will scatter with a very small S -matrix, $s \ll 1$. We would then expect $h s^m i \ll h s i$ when $m > 1$. In fact, if one assumes that $h s^{m+1} i \sim h s^m i$ for sufficiently large Y , then one gets from Eq. (2.14)

$$h s^m i_{MFA} \sim e^{-mY} \quad \text{for large } Y; \quad (3.2)$$

which is indeed consistent⁷ with the initial assumption $h s^{m+1} i \sim h s^m i$ (at least, as long as $m \neq 1$), but is nevertheless in contradiction with the correct asymptotic behaviour exhibited in Eq. (3.1). The problem with the estimate (3.2) is that it is based on a kind of mean field approximation that implicitly assumes that the average S -matrix is controlled by the *typical* configurations in the target, which have a large density. In reality, however, even at very large Y there is still a non-vanishing probability that dilute configurations remain present in the target. As we shall show explicitly, the sum over n in Eq. (2.13) is dominated, at large Y , by *rare fluctuations* for which n is relatively low, $n \ll O(1)$, and therefore $s \sim n \ll 1$, which in turn

⁷ But, clearly, this self-consistency disappears for large $m > 1$, which explains why the Ansatz (3.2) cannot be a solution to the complete hierarchy. In fact, because of the coupling between small and large values of m throughout the hierarchy, the estimate (3.2) is wrong even for relatively small $m \geq 2$, as clear from the comparison with Eq. (3.1).

implies $s^m \approx s$. Such fluctuations have a low probability, $\exp(-Y)$, but this is more than compensated by the fact that their contribution to the average S -matrix is relatively large, of order one. The typical configurations, on the other hand, have a probability of order one, but for them n is very large, of the order of the average number of dipoles in the target, which at large Y is $\ln(1 + (Y - Y_c))$ (see Eq. (2.23)). As a result, the contribution of these configurations to $\langle s^m \rangle$ is exponentially suppressed when $Y - Y_c \gg m/n \approx \exp(-m/Y)$. These simple estimates suggest that, at least for $m \geq 2$, the average S -matrix $\langle s^m \rangle$ should be fully dominated by the rare configurations which are dilute. The case $m = 1$ is a priori more subtle, since then both rare and typical configurations could bring significant contributions.

To make this discussion more quantitative and confirm the asymptotic behaviour displayed in Eq. (3.1), we shall now proceed to an explicit calculation of the probabilities $P_n(Y)$. We do so by using the Laplace transform of $P_n(Y)$

$$\mathcal{P}_n(s) = \int_0^\infty dY e^{-sY} P_n(Y); \quad (3.3)$$

in terms of which the master equation reads

$$\mathcal{P}_n(s) = \frac{f_{n-1} \mathcal{P}_{n-1}(s) + P_n(0)}{s + f_n}; \quad (3.4)$$

Using the initial condition $P_n(0) = \delta_{n1}$, we get

$$\mathcal{P}_n(s) = \frac{1}{f_n} \sum_{k=1}^n \frac{f_k}{s + f_k}; \quad (3.5)$$

from which one can obtain $P_n(Y)$ by the inverse Laplace transform

$$P_n(Y) = \frac{1}{2\pi i} \oint_C ds e^{sY} \mathcal{P}_n(s); \quad (3.6)$$

where the integration is to be done in the counterclockwise direction along any contour C enclosing all the poles of $\mathcal{P}_n(s)$. Notice that all these poles occur in the finite interval $(-1; 1]$.

There are two limiting behaviors of $P_n(Y)$ that can be identified respectively with the cases of weak coupling ($f_n = n$) and strong coupling ($f_n = 1$). In the first case one obtains the familiar distribution of the dipole model [3]

$$P_n^{\text{dip}}(Y) = e^{-Y} \sum_{k=1}^n \frac{Y^{k-1}}{(k-1)!}; \quad (3.7)$$

In the second case, the distribution is of the Poisson type:

$$P_n^{\text{Poisson}}(Y) = \frac{Y^{n-1}}{(n-1)!} e^{-Y}; \quad (3.8)$$

In the general case, we do not have a closed expression but one can easily construct $P_n(Y)$ in the form of a (finite) sum:

$$P_n(Y) = \sum_{k=1}^{X^n} c_k^n e^{f_k Y}; \quad (3.9)$$

with coefficients c_k^n determined by

$$\sum_{k=1}^{X^n} c_k^n = 1 \quad \text{and} \quad c_k^n = \frac{f_{n-1}}{f_n - f_k} c_{k-1}^n; \quad (3.10)$$

These can be iteratively constructed. Here we shall present only few of them, some of which will be important for our subsequent analysis. We have

$$c_1^n = \frac{1}{n-1}; \quad c_2^n = \frac{f_{n-1}}{2n-3}; \quad \dots; \quad c_{n-1}^n = \frac{(1)^{n-1} f_{n-1}}{n(n-1)=2}; \quad c_n^n = \frac{(1)^{n+1}}{n(n-1)=2}; \quad (3.11)$$

Just for illustration, the first four probabilities are given by

$$P_1(Y) = e^Y; \quad (3.12)$$

$$P_2(Y) = \frac{1}{2} e^Y - \frac{1}{2} e^{f_2 Y}; \quad (3.13)$$

$$P_3(Y) = \frac{1}{2} e^Y - \frac{1}{3} \frac{1}{(1-f_2)^2} e^{f_2 Y} + \frac{1}{3} e^{f_3 Y}; \quad (3.14)$$

$$P_4(Y) = \frac{1}{3} e^Y - \frac{1}{5} \frac{1}{(1-f_2)^3} e^{f_2 Y} + \frac{1}{6} \frac{1}{(1-f_3)^3} e^{f_3 Y} - \frac{1}{6} e^{f_4 Y}; \quad (3.15)$$

It is easy to verify that these distributions go over to either the dipole distribution (3.7) or the Poisson distribution (3.8) as $\beta \rightarrow 1$ or $\beta \rightarrow 0$, respectively.

From Eq. (3.9)–(3.11), it is clear that for large Y and not too large values of n , the dominant contribution to $P_n(Y)$ is given by the first term in Eq. (3.9), proportional to e^Y . Indeed, the terms with $k \geq 2$ are exponentially suppressed at large Y with respect to the first term. But the situation changes when n becomes large, since the coefficients c_k^n increase rapidly with n and this rise can compensate for the exponential suppression with Y . One can roughly estimate the value of n at which this change of regime occurs by requiring that the first two terms in the expansion of $P_n(Y)$ become of the same order. This criterion yields

$$n_{cr} = \frac{Y}{\ln(1-\beta)} - \frac{Y}{Y_c}; \quad (3.16)$$

where $Y_c = \ln(1-\beta)$, as before, and the second estimate holds when $\beta \rightarrow 1$. A more precise estimate for n_{cr} will be obtained in the next section and reads $n_{cr} = (\beta - 1)Y / \ln \beta$. Clearly, this number is of the order of, but smaller than, the average number of particles $\ln n$ at large Y (cf. Eq. (2.23)). Hence, the configurations with $n < n_{cr}$ are relatively *dilute* and thus have a small probability, approximately given by the first term in the sum in Eq. (3.9): $P_n(Y) \approx (1-\beta)^{n-1} e^Y$. In Fig. 1, this analytic estimate is compared with the exact result, as obtained by numerical integration in the master equation. On the other hand, for $n > n_{cr}$ — the case of the *typical* configurations — $P_n(Y)$ is of order one and is dominated by the terms with large values of k , of order n (see Sect. 3.2). As discussed above, we do not expect these

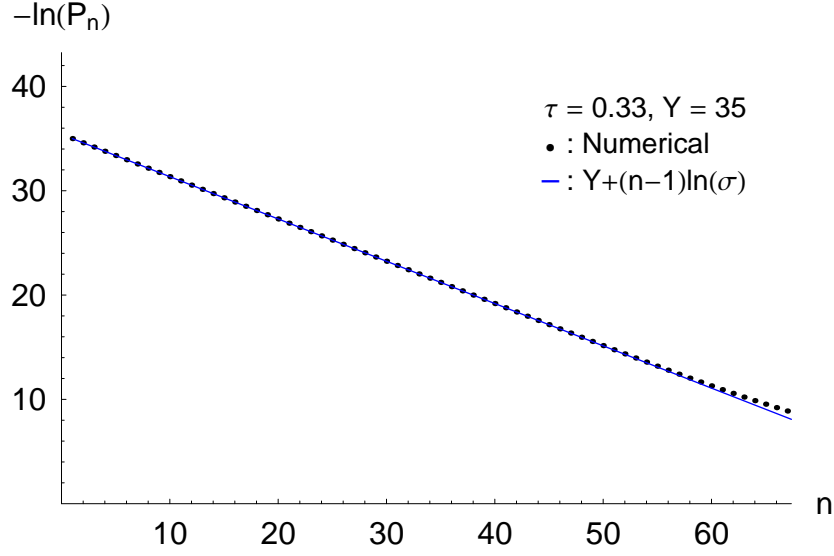


Fig. 1. For high Y and values of n such that $n \gg n_{\text{cr}}$ the probabilities $P_n(Y)$ are dominated by the first term of the sum in Eq. (3.9). Notice that for the values of Y and σ used in this plot, $n_{\text{cr}} \approx 67$.

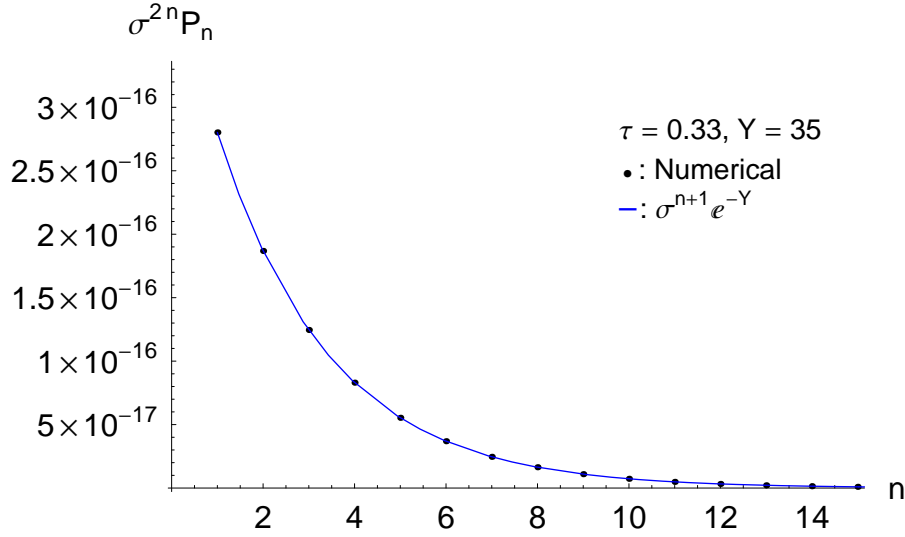


Fig. 2. The distribution $\sigma^{2n}P_n$ as a function of n for large Y ; only the rare configurations with n up to $n_{\text{cr}} \approx 67$ contribute to $\langle h^2 \rangle$.

bulk configurations to affect the calculation of the average S-matrix elements $\langle h^m \rangle$, which are expected to be controlled by the dilute configurations with $n \ll n_{\text{cr}}$.

Let us verify this by explicitly computing $\langle h^m \rangle$, starting with $m = 2$. To that aim, we separate out the contribution of the configurations with $n \ll n_{\text{cr}}$ in Eq. (2.13) for $\langle h^2 \rangle$. This yields

$$\langle h^2 \rangle = \sum_{n=1}^{n_{\text{cr}}} P_n(Y) \sigma^{2n} e^{-Y} \frac{n_{\text{cr}}}{n-1} = \frac{1 - \sigma^{2(n_{\text{cr}}-1)}}{1 - \sigma^2} e^{-Y} \approx \frac{1}{1 - \sigma^2} e^{-Y}; \quad (3.17)$$

where the neglected terms are of $O(\sigma^{2(Y - Y_{\text{cr}})})$, and thus are exponentially suppressed when

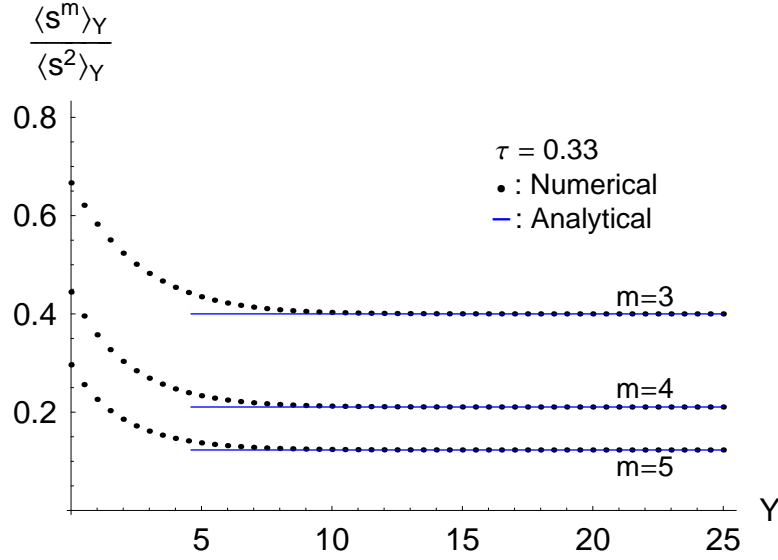


Fig. 3. The S-matrix for the scattering of m projectile dipoles normalized to that for the scattering of two dipoles; for $Y = Y_c = 1.5$ and $m = 2$, the Y -dependence is the same and equal to e^Y .

$Y = Y_c$ relatively to the dominant contribution, of $O(e^{(Y-Y_c)})$. In practice only the configurations with up to $l = 1$ dipoles contribute to the final result (this is manifest in Fig. 2), and for them $n > l = 1$ e^1 . For any such configuration, the S-matrix for a projectile dipole is of order one, $s = n = O(1)$, as anticipated. The contribution of the bulk configurations with $n > n_{cr}$ to hs^2i will be considered in Sect. 3.2 and found to be of $O(e^{2(Y-Y_c)})$, so like the terms neglected in evaluating Eq. (3.17). Hence, the final result in Eq. (3.17) gives indeed the dominant behaviour when $Y = Y_c$.

Clearly that one can extend this calculation to an arbitrary $m = 2$. In fact, the larger is m , the faster is the convergence of the sum over n in Eq. (2.13) works⁸. It is then straightforward to show that

$$hs^m i = \frac{1}{m-1} e^Y \quad \text{for } m = 2 : \quad (3.18)$$

We emphasize here that not only the Y -dependence, but also the prefactor in the above equation are well under control. This result is in agreement with the respective one in Eq. (3.1) and it fixes the parameter A there to be $A = 2$. More generally, the above procedure allows one to estimate the generating functional $Z(u; Y)$, Eq. (2.9), for large Y and any value of u which is strictly smaller than 1 : the corresponding result is obtained by replacing $m = 1$ by u in Eq. (3.18) (see also Appendix B). The analytic estimate (3.18) for $hs^m i$ and the corresponding one for $Z(m) = Z(u = m)$ are compared to the respective numerical results in Figs. 3 and 4.

Let us now turn to the case $m = 1$, which is special. The analog of Eq. (3.17) reads then

$$hsi = \sum_{n=1}^{\infty} P_n(Y) e^Y = \sum_{n=1}^{\infty} \frac{1}{n} (Y - Y_c) e^Y ; \quad (3.19)$$

⁸ The extreme limit of this behavior occurs when m becomes larger than $l = 1$. Then the only configuration of the target wavefunction which is relevant is the one with $n = 1$.

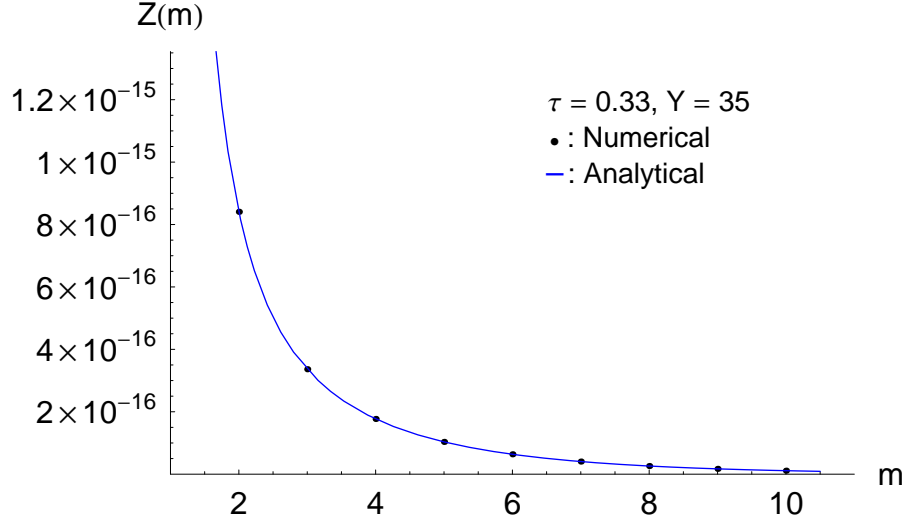


Fig. 4. The generating functional as a function of $m = \ln u = \ln$ for $m > 1$. When m is an integer, $Z(m)$ gives the S-matrix for the scattering of m projectile dipoles off the target.

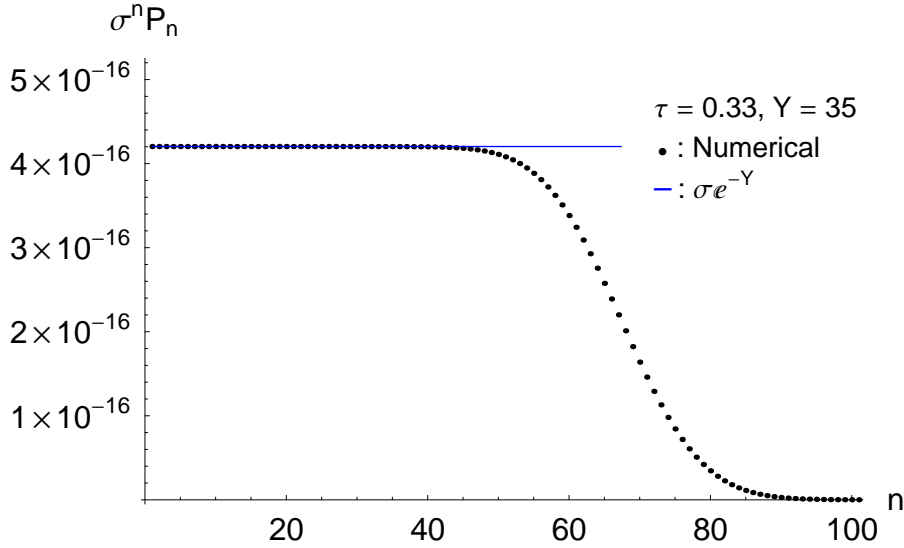


Fig. 5. The distribution $\sigma^n P_n$ as a function of n for large Y ; all the configurations with n up to n_{cr} ($Y - Y_c =$ contribute to hsi.

where we have used the improved estimate $n_{cr} = (Y - Y_c)$, to be found in Sect. 3.2. The prefactor in front of the exponential in the final result is essentially the number of configurations which contribute to the average S-matrix, with each such a configuration bringing a contribution of $O(e^{-Y})$. Note, however, that the above sum is dominated by its upper limit, i.e., by configurations with $n \approx n_{cr}$, for which our approximations are not fully under control. This result turns out to be nevertheless correct (up to corrections of $O(1)$ to the rapidity shift Y_c , which go beyond the present accuracy), for the following reason: the distribution $\sigma^n P_n(Y)$ is almost flat as a function of n so long as $n \leq n_{cr}$ — as manifest on Eq. (3.19) — but it drops out very fast when $n > n_{cr}$ (this can be seen in the numerical results in Fig. 5 and will be

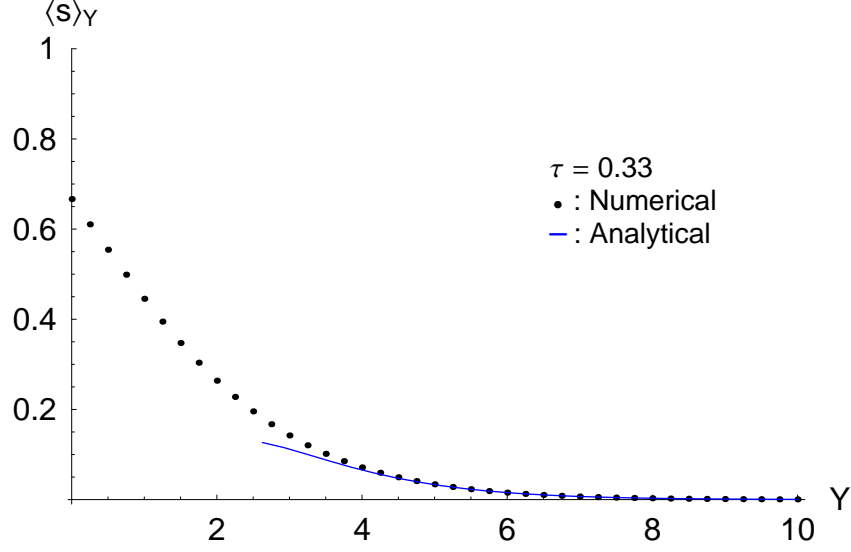


Fig. 6. The expectation value $\langle S \rangle_Y$ of the S -matrix for onium-onium scattering. Starting from $\langle S \rangle_0 = 1$, this expectation value falls exponentially to zero when $Y \gg Y_c$, in agreement with the analytic prediction (3.19) (see also Fig. (7)).

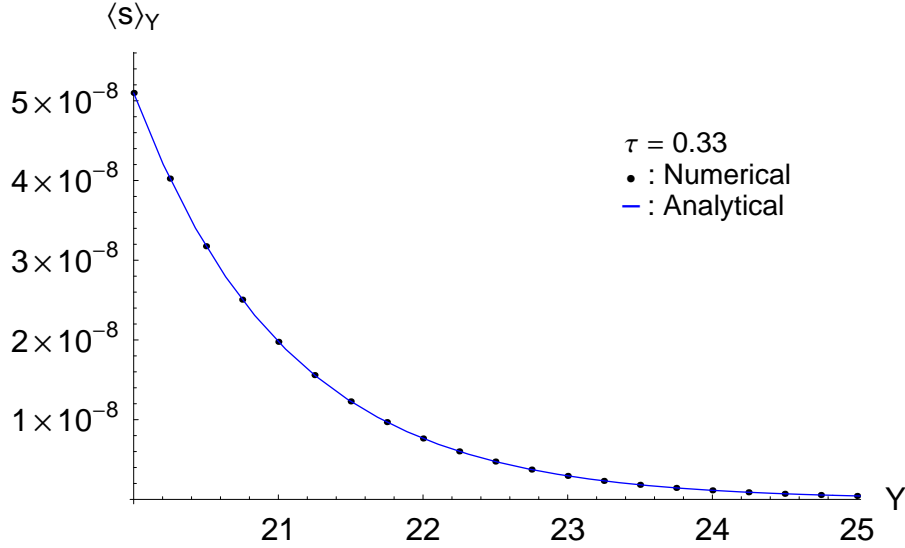


Fig. 7. The average value $\langle S \rangle_Y$ for higher values of Y . The analytic curve is obtained by using Eq. (3.19) with $Y_c = \ln(1/\tau)$.

analytically verified in the next section).

A different way to check Eq. (3.19) is to rely on the hierarchy of evolution equations for $\langle S \rangle_Y$. As previously noticed, $\langle S \rangle_Y$ given by Eq. (3.18) is an accurate asymptotic solution for all the equations in the hierarchy starting with the second one. Then one can use this result, together with the first equation in the hierarchy, Eq. (2.15), in order to determine the asymptotic form of $\langle S \rangle_Y$. Thus one easily recovers Eq. (3.19) where however the rapidity shift Y_c is left undetermined. A further confirmation of Eq. (3.19) can be found in the original calculation of $\langle S \rangle_Y$ by Mueller and Salam [1], which is based on the solution to Eq. (2.17) and which yields

the same result as our Eq. (3.19) with $Y_c = \ln(1/\epsilon) + O(1)$. The analytic estimate (3.19) is compared to the respective, exact, numerical result in Figs. (6) and (7), which confirm that both the Y -dependence and the normalization shown in Eq. (3.19) are indeed under control.

To conclude this section, it is instructive to compare the above results to those predicted by the dipole picture. Since the latter is inconsistent with boost invariance, we shall obtain different results for h_s^m depending upon the system that we decide to evolve: the target or the projectile:

(i) *Projectile evolution in the dipole picture.* The dipole S -matrix elements h_s^m obey the Balitsky equations, that is, Eq. (2.14) with the prefactor f_m replaced by m . By doing this replacement, one loses Lorentz invariance. This is formally recovered by allowing the projectile and the target to obey different evolution equations. Namely, if the projectile obeys dipole evolution, then in order for the r.h.s. of Eq. (2.12) to be independent of Y_0 , the target probabilities $P_n^R(Y - Y_0)$ which enter $h_s^m(Y - Y_0)$ via Eq. (2.13) must evolve according to the ‘JIMWLK’ version of the master equation⁹, i.e., Eq. (2.17).

Let us then estimate the high-energy behaviour of h_s^m as predicted by the Balitsky equations: by inserting the Ansatz $h_s^m = \exp(-c_m Y)$ in this hierarchy, one immediately finds $c_m = m$, and hence

$$h_s^m = e^{-mY} \quad \text{at large } Y \quad (\text{no saturation in the projectile}) ; \quad (3.20)$$

which is essentially the mean field estimate (3.2). Thus, by neglecting saturation effects in the projectile wavefunction (or, equivalently, particle-number fluctuations in the target wavefunction), we are led to the wrong conclusion that h_s^{m+1} vanishes faster than h_s^m at large Y .

(ii) *Target evolution in the dipole picture.* By using the target-average expression (2.13) for h_s^m together with the explicit solution (3.7) for the probabilities in the dipole picture, one immediately finds:

$$h_s^m \sim \frac{m}{1-m} e^{-Y} \quad \text{for } m < 1 \text{ and large } Y \quad (\text{no saturation in the target}); \quad (3.21)$$

where the neglected terms are of order $O(e^{-2Y})$. For $m = 2$, this is essentially the same as the correct result at large Y , as given in Eq. (3.18). This agreement is consistent with the fact that h_s^m with $m = 2$ is dominated by rare target configurations which have a low density and thus are insensitive to saturation effects. For $m = 1$, on the other hand, the dipole-picture prediction in Eq. (3.21) is quite different from the correct respective result in Eq. (3.19); namely, it misses the large, overall, factor $Y - Y_c$, which in Eq. (3.19) has been produced by summing over configurations with a relatively large number of particles $n < (Y - Y_c) =$ (cf. Eq. (3.19)), which are close to saturation.

3.2 The bulk of the particle distribution

Although quasi-irrelevant for the calculation of the average S -matrix at high energy, as we have just seen, the typical configurations are nevertheless interesting in that they determine the distribution of the bulk of the particles at high energy. In what follows, we shall study the

⁹ This is, of course, in agreement with the fact that the reduced Balitsky equations (2.18) can be also obtained from the ‘JIMWLK’ evolution (2.17) of the target.

probability distribution $P_n(Y)$ at high energy (typically, $Y \gg \ln(1=)$) and for a large number of particles $n \rightarrow \infty$, which we anticipate to be the case for the typical configurations.

To compute this distribution, we return to the exact Laplace transform, Eq. (3.5), and write

$$\ln [f_n \mathbb{P}_n(!)] = \sum_{k=1}^{\infty} \ln \left(1 + \frac{!}{f_k} \right) = \sum_{r=1}^{\infty} \frac{(-1)^{r+1}}{r} \sum_{k=1}^{\infty} f_k^{-r} ; \quad (3.22)$$

where we have expanded the logarithm and exchanged the order of the two summations. We shall now perform the summation over k in the above equation, under the assumptions that $n \rightarrow \infty$ and $! \rightarrow \infty$. More precisely, we shall neglect terms which are of order (or smaller than) $O(e^{-n})$ and/or $O(1/n)$. Notice that all these summations grow linearly with n for large n (since $f_k^{-r} \sim e^{-rk}$ when $k \rightarrow \infty$), so it will be convenient to subtract this large contribution and then perform approximations on the remainder. We thus have

$$\sum_{k=1}^{\infty} f_k^{-1} = \sum_{k=1}^{\infty} \frac{1}{1 - e^{-k}} \sim n + \sum_{k=1}^{\infty} \frac{e^{-k}}{1 - e^{-k}} \sim n + \ln(1=) + \gamma ; \quad (3.23)$$

where the third, approximate, equality has been obtained by extending the upper limit of the sum from n to ∞ , which is correct up to terms of order $O(e^{-n})$. The ensuing sum is evaluated in Appendix C under the assumption that $n \rightarrow \infty$. Also, $\gamma = 0.577\ldots$ is the Euler constant.

Similarly for $r \geq 2$ we have (cf. Appendix C)

$$\sum_{k=1}^{\infty} f_k^{-r} = \sum_{k=1}^{\infty} \frac{1}{(1 - e^{-k})^r} \sim r n + \sum_{k=1}^{\infty} \frac{(1 - e^{-k})^{-r}}{(1 - e^{-k})^r} \sim r n + \zeta(r) ; \quad (3.24)$$

where $\zeta(r)$ is the Riemann Zeta function. Note that the above summations are dominated by large values $k = O(n)$, as anticipated in the discussion preceding Eq. (3.16). Using Eqs. (3.23) and (3.24), one can do the summation over k in Eq. (3.22) to obtain

$$\ln [f_n \mathbb{P}_n(!)] \sim ! \ln(1=) - n \ln(1 + !^{-1}) + \ln(1 + !^{-1}) ; \quad (3.25)$$

Thus we finally arrive at

$$P_n(Y) \sim \int_0^{\infty} \frac{d!}{!} \frac{e^{! [Y - \ln(1=)]} (1 + !^{-1})}{(1 + !^{-1})^n} ; \quad (3.26)$$

which so far is valid for large $n \rightarrow \infty$ but arbitrary Y . It is straightforward to check that this distribution satisfies indeed the large- n version of the master equation, i.e., the equation obtained from Eq. (2.3) after replacing $f_n \rightarrow 1=$, as appropriate when $n \rightarrow \infty$.

Even though Eq. (3.26) is considerably simpler than the general form, it is still difficult to proceed without any further approximations, because of the presence of the Gamma function which has single poles on the negative real axis. Since we are interested in large values of n and Y , we can evaluate the integral in Eq. (3.26) using a saddle point approximation. As we shall see, the saddle point will occur at a small value of $!$, so that we can replace the Gamma function by the lowest order terms in its expansion around $! = 0$: $(1 + !^{-1})^{-n} \sim 1 - n!^{-1}$. (This means that only the sum $\sum_{k=1}^{\infty} f_k^{-1}$ in Eq. (3.23) and the $r n$ terms of the sums in Eq. (3.24) are kept in the subsequent analysis.) We then obtain

$$P_n(Y) = \frac{1}{2\pi i} \oint_C \frac{d!}{2} \frac{e^{-!}}{(1+!)^n} = \frac{1}{2\pi i} \oint_C \exp[F(!_0)]; \quad (3.27)$$

where we have defined the variable

$$! = \frac{Y}{n} \ln(1+); \quad (3.28)$$

and the function

$$F(!) = ! - n \ln(1+!); \quad (3.29)$$

while the contour integral over $!$ has been evaluated in the saddle point approximation. For the latter to be justified, at least one of the conditions $! \ll 1$ (i.e., $Y \ll n \ln(1+)$) and $n \gg 1$ needs to be satisfied. Besides, the saddle point must obey $|!_0| \ll 1$, for consistency with the previous manipulations. Clearly, the saddle point occurs at

$$!_0 = \frac{n}{Y}; \quad (3.30)$$

so the condition $|!_0| \ll 1$ is tantamount to $n \gg j$. Evaluating F and F' at the saddle point¹⁰ and substituting in Eq. (3.27) we finally obtain a Poisson distribution, as anticipated:

$$P_n() = \frac{1}{(n)} n^{-1} e^{-} : \quad (3.31)$$

As aforementioned, this approximation is valid so long as $j \ll n$. This range covers indeed the “bulk” of the distribution at large Y (see also Fig. 8): when summed over n within this range, Eq. (3.31) yields a total probability equal to 1 up to terms of order $O(e^{-})$. Moreover, the lower limit $n_{\text{min}} =$ is essentially the same as the upper limit (previously denoted as n_{cr}) of the validity range of the approximation for P_n constructed in Sect. 3.1 (which, we recall, consists in preserving only the first term in the sum in Eq. (3.9)). Indeed, if one redefines n_{cr} via the condition that these two approximations match with each other (up to prefactors) when $n = n_{\text{cr}}$, then one finds $n_{\text{cr}} = (1 + O(2)) n_{\text{min}}$. Thus, the two approximations for P_n at large Y that we have constructed in this paper are complementary to each other, in the sense that, together, they cover all the interesting values of n and they approximately match with each other at the borderline $n_{\text{min}} \approx n_{\text{cr}}$ between their respective domains of validity in n .

Now let us discuss some aspects of this distribution. The maximum of the distribution occurs at $n = + 1=2$ and the value at the maximum is $P_n = P_{\text{max}} = 1=2$, while the width of the distribution is proportional to P^{-} . We need to say here that terms of order $O(\ln(1=))$ in the location of the maximum have not been kept, since this would requires a calculation of $_{-1}$ in Eq. (3.23) to $1=$ accuracy (see Appendix C).

From Eq. (3.31) is is straightforward to deduce the average particle number at high energy — one thus finds $\langle n \rangle =$, which is indeed the same as in Eq. (2.23) — and, more generally, all

¹⁰ Notice that the saddle point conditions require that the integration contour crosses perpendicularly the real axis.

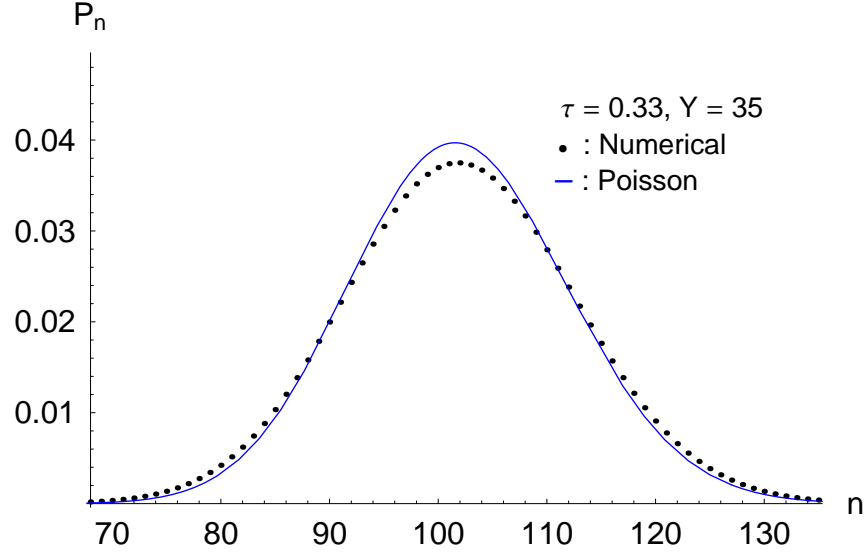


Fig. 8. For high Y the probabilities $P_n(Y)$ follow a Poisson distribution for large values of n .

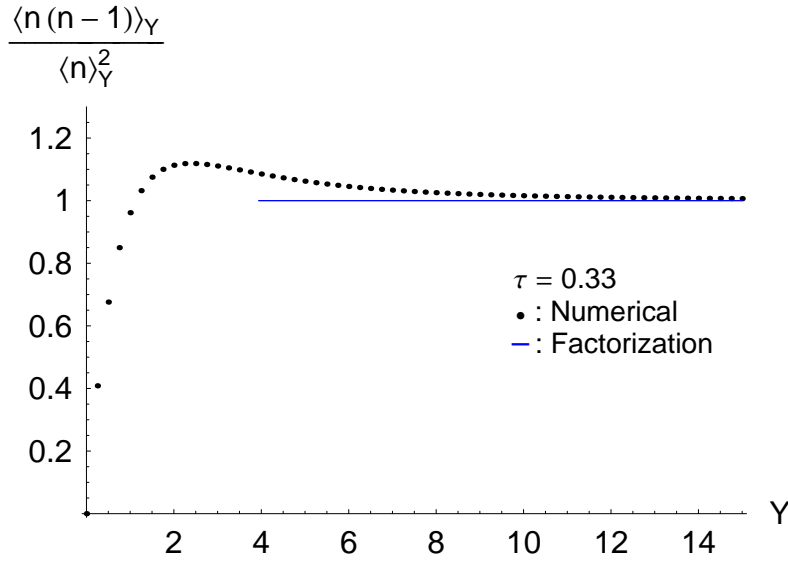


Fig. 9. Factorization of expectation values holds only for quantities dominated by the bulk of the probability distribution; here the ratio of the (normal ordered) pair density with respect to the single density squared which approaches unity for $Y \gg Y_c$, in agreement with Eq. (3.32).

the k -body dipole densities, which are readily obtained as ¹¹

$$\ln^{(k)} i = \ln i^k = k \quad \text{when} \quad Y \gg Y_c : \quad (3.32)$$

This equation exhibits mean-field-like factorization, as expected for the bulk distribution at high density ¹². This is illustrated in Fig. 9.

¹¹ We should mention here that the calculation of $\ln^{(k)} i$ is consistent with the validity range of the distribution (3.31) only so long as $k \ll 1$.

¹² Notice that this is not the factorization that one finds in the dipole picture, i.e., in the absence of

Finally, let us use the Poisson distribution (3.31) to compute the contribution of the bulk configurations to the expectation value of the S -matrix for the scattering of m external dipoles. One thus finds

$$\ln \langle i_{\text{bulk}}^m \rangle = \sum_m e^{-f_m} \ln f_m; \quad (3.33)$$

as expected from the mean field approximation, cf. Eq. (3.2). However, for $m \geq 2$, this bulk contribution is exponentially smaller (at large $Y \gg Y_0$) than the respective contribution of the rare configurations with only few particles, as previously computed in Eq. (3.18). Also, even for $m = 1$, the result above is smaller by a large factor $1 = (Y_0/Y)^{1/2}$ than the previous result in Eq. (3.19), which, we remember, is due to the configurations with $n < n_{\text{cr}}$. Thus, the present calculation of the bulk distribution confirms our previous conclusion that the S -matrix is dominated by the rare configurations which involve relatively few particles.

4 Correspondence between the toy model and high energy QCD

Throughout this paper, we have already emphasized at several places some similarities between the structure and the behaviour of the toy model and some known, or expected, properties of high-energy QCD. In what follows, we shall discuss this correspondence in a more systematic way, with the purpose of demonstrating the following point: in spite of the limitations inherent in the toy model, as associated with the lack of transverse dimensions, this model shares nevertheless some fundamental structural properties with the corresponding QCD problem, hence its analysis may lead to conceptual clarifications in view of the considerably more involved problem of real QCD.

Let us start with the factorization formula for the S -matrix, Eq. (2.1), which lies at the heart of the toy model. This formula is reminiscent of the factorization schemes proposed within high-energy QCD in Refs. [3, 11, 22, 23, 48], which have in common to be symmetric between the projectile and the target. With the noticeable exception of the dipole factorization [3], which however fails to accommodate the saturation effects in the wavefunctions of the colliding hadrons, all the other schemes alluded to above are not written in terms of particle numbers, but rather in terms of gluon fields, sometimes represented (in the CGC formalism [37]) as classical color charges together with the color fields they radiate. It is therefore essential to establish the proper correspondence between gluons in QCD and particles in the toy model.

This correspondence goes as follows: the ‘dipoles’ in the toy model correspond to gluons in the s -channel in QCD (so like the actual, color, dipoles in Mueller’s dipole picture for QCD), whereas the factors of $1 = 1$ correspond to gluons exchanged in the t -channel. (The analog of 1 in QCD starts at order s^2 , corresponding to a two-gluon exchange between a pair of dipoles.) Hence, in an effective gluon language, the evolution described by Eqs. (2.3) and (2.5) contains vertices for gluon splitting in the s -channel — these are, of course, the vertices f_n — and also vertices for both splitting and merging in the t -channel — each exchange being sandwiched between two such vertices. Hence, this evolution constructs the analog of the ‘Pomeron loops’ in the onium wavefunction. Fully symmetric ‘Pomeron loops’ will develop, of course, in the S -matrix for onium–onium scattering, as described by Eq. (2.1).

saturation; in that case one rather has $\ln \langle i^{(k)} \rangle \sim k \ln i^k$ at large Y [3].

With this identification, the toy-model hierarchy for the dipole scattering amplitudes, cf. Eqs. (2.14) or (2.19)–(2.21), corresponds to the QCD evolution equations with Pomeron loops, as constructed in Refs. [17–19]. To render this analogy more precise, let us first focus on the limiting case in which the evolutions of the projectile and the target are treated dissymmetrically, so that the Pomeron loops are in fact absent (this would correspond to Balitsky–JIMWLK approximation to the high-energy evolution in QCD). We have already noticed in Sect. 2.2 that, in this approximation — which neglects the saturation effects in the wavefunction of the projectile or, equivalently, the particle-number fluctuations in that of the target —, the general evolution equations (2.14) reduce to the (zero-dimensional version of the) Balitsky equations. Since, within QCD, the latter equations can be also obtained from the JIMWLK evolution of the target, we expect the continuum version of the master equation, i.e., Eq. (2.17), to be the toy-model analog of the JIMWLK equation in QCD.

Let us explain here this analogy in more detail: the JIMWLK equation [7–9] is written for the color fields A_a^+ radiated in the t -channel by the gluons produced in the s -channel by the high-energy evolution of the (right-moving) target. It is a second-order, functional, differential equation with respect to A_a^+ and reads, schematically,

$$\frac{\partial W_Y[\dots]}{\partial Y} = \frac{1}{2} \frac{\partial^2}{\partial A_a^+ \partial A_b^+} K^{ab}[\dots] W_Y[\dots]; \quad (4.1)$$

where the transverse coordinates have not been shown. The quantity $W_Y[\dots]$ is the probability distribution for the fields A_a^+ (the analog of $P_n(Y)$ of the toy model). The kernel $K^{ab}[\dots]$ — the analog of the emission rate f_n — is non-linear in A_a^+ to all orders, via Wilson lines which describe the multiple scattering of the gluon which is emitted in the s -channel in the last step of the evolution off the background field A_a^+ produced in the t -channel by the previous evolution; clearly, this rescattering is similar to that included in f_n within the toy model. To complete the identification between Eqs. (4.1) and (2.17), one should also keep in mind that, in the approximations underlying the JIMWLK equation, each s -channel gluon is allowed to radiate only two gluons in the t -channel. Hence, the second-order derivative w.r.t. A_a^+ in Eq. (4.1) can be roughly interpreted as a single derivative w.r.t. n (the number of gluons in the s -channel); with this interpretation, Eq. (4.1) becomes indeed formally similar to Eq. (2.17).

Strictly speaking, the JIMWLK equation *does* include some fluctuations, as obvious from the fact that it is a second-order differential equation — i.e., a Fokker–Planck equation for a random walk (here, a walk in the functional space of color fields [10]). However, these are merely *color* fluctuations, and are suppressed at large N_c . But the essential correlations associated with *gluon-number* fluctuations are lost because of the impossibility to probe both (s -channel) gluons which are produced after one splitting. This is related to the fact that, as aforementioned, an s -channel gluon cannot radiate more than two t -channel fields, and thus cannot undergo multiple scattering off the projectile. By contrast, within the toy model, the dipoles *are* allowed to scatter multiply — both inside the target wavefunction and with the dipoles in the projectile —, hence the n -body correlations associated with splitting are fully taken into account. In the language of QCD, each s -channel gluon is allowed to absorb and radiate an arbitrary number of t -channel gluons, so like in the more general, ‘self-dual’, evolution described in Refs. [24, 25].

In fact, as noticed in Ref. [33], the structure of the master equation for the toy model bears some formal resemblance to that of the ‘diamond’ Hamiltonian constructed in Refs. [24, 25];

in particular, it shares with the latter the property of being self-dual, as it should (since the self-duality of the evolution Hamiltonian is equivalent with the condition of boost-invariance for the S -matrix whenever the latter can be factorized like in Eq. (2.1) [22, 23]). To see this, note that the master equation can be formally rewritten as (cf. Eqs. (2.3) and (2.5))

$$\frac{dP_n(Y)}{dY} = \frac{1}{n} \left(1 - e^{\frac{\partial}{\partial n}} \right) \left(1 - e^{n j \ln j} \right) P_n(Y) - H n j \ln j \frac{\partial}{\partial n} P_n(Y); \quad (4.2)$$

where we have extended n to be a continuum variable (whose interesting values are the positive integers though) and used $g(n+1) = \exp \int d\ln g g(n)$ for a generic function $g(n)$. As anticipated, the ‘Hamiltonian’ appearing in Eq. (4.2) is ‘self-dual’ [33], that is, it is invariant under the self-duality transformation which in the present context consists in exchanging

$$\frac{\partial}{\partial n} \rightarrow n j \ln j; \quad (4.3)$$

and then reversing the order of the operators. Moreover, the presence of two types of exponentials — one involving the number n of particles, the other one, the derivative $\partial/\partial n$ with respect to this number — is reminiscent of the two types of Wilson lines which appear in the QCD Hamiltonian proposed in Refs. [24, 25]. In QCD, $n j \ln j$ is replaced by the color field produced by the s -channel gluons, and $\partial/\partial n$ by the (functional) derivative with respect to the color charge density of these gluons.

Let us now return to the equations obeyed by the dipole scattering amplitudes and compare the structure of the fluctuation terms between the toy model and QCD. Consider first the equation for h^2 , as displayed in Eq. (2.20) for the toy model and, respectively, in Eqs. (2.7) and (2.8) of Ref. [18] for QCD. In both cases, the dominant fluctuation term is of the generic type h , i.e., it is linear in h and of order $\frac{2}{s}$. Yet, the experience with the toy model tells us that the coefficient of the fluctuation term in QCD (cf. Eq. (2.7) in Ref. [18]) may actually be incomplete. Indeed, in the calculation of this term in Refs. [17–19] one has neglected the possibility that the individual dipoles from the target undergo multiple scattering with the dipoles in the projectile; that is, in deriving the equation for h^2 , the two external dipoles have been allowed to scatter only with two *different* dipoles from the target (but not also to scatter both off a *same* dipole). By contrast, in the respective toy model calculation, multiple scattering *is* included and is in fact responsible for an $O(1)$ contribution to the coefficient of fluctuation term h in Eq. (2.20): if that contribution was neglected, the ensuing coefficient would be twice as large than the correct one.

More generally, if one considers the equation satisfied by h^m within the toy model, then among the $m-1$ (relevant) fluctuation terms which are included in this equation (cf. Sect. 2.2) — namely, h^{m-1} , h^{m-2} , ..., h — only the analog of the first term, h^{m-1} , has been so far included in the corresponding equation in QCD [18]. The other terms, which are missing in QCD, come again from the multiple scattering of the individual target dipoles — a process which should also affect the coefficient of the first term as compared to its original calculation in QCD.

This discussion allows us to draw some lessons from the toy model in view of QCD: most likely, the Pomeron loop equations in QCD at large N_c should be completed by including the effects of the multiple scattering of the individual target dipoles. This conclusion appears to be in conflict with some recent analyses within QCD [49, 50], which should be therefore carefully

reexamined. Furthermore, the more intricate structure for the fluctuation terms suggested by the toy model seems to prevent one from mapping the problem under study — in either the toy model, or in QCD — into a single Langevin equation.

But although the detailed structure of the fluctuation terms in QCD may be indeed more complicated than anticipated by the original analysis in Refs. [17–19, 23], we do not expect such additional terms, if any, to modify the qualitative, asymptotic, behaviour of the dipole scattering amplitudes at high energy (and large N_c) : as argued in Refs. [15, 17], this behaviour is rather dictated by universal properties of the stochastic evolution equations.

An other interesting result of the toy model that we expect to extend to QCD as well is the fact that the average S -matrix in the vicinity of the unitarity limit is dominated by rare fluctuations with only few gluons. This is in agreement with the arguments presented in that sense in Refs. [1, 12] (in the context of QCD), which also show that the exponential approach towards the black disk limit should be somehow faster in QCD, namely like¹³ $h_{\text{si}} \sim \exp(-Y^2)$, to be compared with the toy-model result $h_{\text{si}} \sim \exp(-Y)$. (The additional factor of Y in QCD comes from the phase-space for diffusion in the dipole transverse sizes.) But what is most interesting about our present results is that the S -matrix h_{sm}^m for the simultaneous scattering of *several* dipoles is even more strongly dominated by the rare fluctuations which are dilute, to the point that h_{sm}^m with $m \geq 2$ is not at all sensitive to saturation effects in the target wavefunction, and (unlike h_{si} !) it could have been simply computed within the dipole picture. It would be interesting to understand whether a similar feature holds in QCD as well. If so, this would mean that, for $m \geq 2$, h_{sm}^m in high-energy QCD at large N_c can be reliably computed via numerical simulations within Mueller’s dipole picture.

Acknowledgments

We would like to thank Al Mueller for useful discussions on the manuscript.

A Lack of boost invariance for the recombination process

In this appendix, we shall consider more general (zero-dimensional) models in which in addition to particle splitting, one allows for recombination. The simplest model of this type is the reaction model $A \rightarrow AA$, introduced in the context of QCD in Ref. [17], and further discussed in Refs. [32, 34, 35]. In that model, a particle can split into two ($A \rightarrow AA$) at a rate \mathcal{F}_1 per particle and, conversely, two particles can recombine into one ($AA \rightarrow A$) with a rate \mathcal{G}_2 per pair of particles. In what follows, we shall consider a more general version of this model, in which the rates for splitting (\mathcal{F}_n) and merging (\mathcal{G}_n) are taken to be general functions of the number n of particles in the system. Hence, in such a process, particle number saturation can in principle occur via two different mechanisms: the saturation of the rate for particle splitting and the particle recombination.

The purpose of this appendix is to show that the recombination process cannot be made consistent with the boost invariance of the S -matrix (within the factorization scheme of Eq. (2.1)) for any choice of the \mathcal{G}_n ’s. This finding, together with the fact that, within the context of the JIMWLK equation, gluon saturation truly occurs via the first mechanism mentioned above

¹³ This is also the behaviour found by Salam, via numerical simulations of the onium–onium scattering within the context of the dipole picture [1, 4].

(i.e., the saturation of the emission rate), suggests that the models including recombination are not relevant in the context of QCD. This conclusion is further supported by the observation in Ref. [26] that, if one attempts to interpret the Pomeron loop equations of QCD [17] as a reaction–diffusion process (in either the target or the projectile), then one is ineluctably driven to an effective ‘recombination vertex’ which has no meaningful probabilistic interpretation.

The master equation is obtained by adding to the r. h. s. of Eq. (2.3) the terms responsible for recombination. We thus obtain

$$\frac{dP_n(Y)}{dY} = f_{n-1} P_{n-1}(Y) - f_n P_n(Y) + g_{n+1} P_{n+1}(Y) - g_n P_n(Y); \quad (\text{A.1})$$

where the functions f_n and g_n should be chosen in such a way to be consistent with the boost invariance of the S –matrix. They satisfy the boundary conditions $f_1 = 0$ and $g_1 = 0$, with the latter meaning the trivial fact that no recombination can happen in a system with only one particle. Once again, we assume the average S –matrix to have the factorized structure in Eq. (2.1). By requiring that it is independent of Y_0 , we easily obtain the following constraint

$$f_m(1-n) - f_n(1-m) - g_n(n-1) + g_m(m-1) = 0; \quad (\text{A.2})$$

A priori, there are two different ways in which this constraint could be satisfied: (i) the independent cancellation of the f –terms and g –terms, and (ii) the mutual cancellation between the two types of terms. As we shall shortly see, they are both excluded.

(i) By requiring the f –terms and, respectively, the g –terms in Eq. (A.2) to cancel independently from each other, one finds

$$f_n = c(1-n) \quad \text{and} \quad g_n = d(n-1); \quad (\text{A.3})$$

where the constant factors c and d are determined by the boundary conditions at $n = 1$. For c , the respective condition yields $c = 0$, which then leads to the expression for f_n that has been used throughout. But the condition $g_1 = 0$ can be satisfied only by choosing $d = 0$, and hence $g_n = 0$ for any n .

(ii) In order for the f –terms to cancel the g –terms in Eq. (A.2) one needs¹⁴

$$f_n = c(n-1) \quad \text{and} \quad g_n = -c(1-n); \quad (\text{A.4})$$

But this solution is meaningless since, depending on the sign of the constant c , either the f_n ’s or the g_n ’s have to be negative, and thus the probabilistic interpretation is lost — a situation reminiscent of the difficulty met in Ref. [26].

The standard reaction–diffusion process $A \rightarrow A A$ is defined by (see, e.g., [17])

$$f_n = n \quad \text{and} \quad g_n = n(n-1)/2; \quad (\text{A.5})$$

and thus it does not belong to the case (ii); this process has a well–defined probabilistic interpretation, but it is inconsistent with the boost invariance of the S –matrix in the factorization scheme of Eq. (2.1), which includes multiple scattering for the individual particles¹⁵.

¹⁴ From the perspective of Eq. (2.1), this would correspond to a scenario in which the emission of a dipole in one onium can be reinterpreted, after a shift in Y_0 , as a recombination in the other onium.

¹⁵ In Ref. [23], the Pomeron loop equations in QCD at large- N_c have been given an effective interpreta-

B Relation with the reaction toy model

In this appendix we shall study the generating functional $Z(u; Y)$ introduced in Eq. (2.9) with two purposes in mind: First, we shall compute its behaviour in the high-energy limit $Y \rightarrow \infty$ (in practice, $Y \gg Y_c$), while paying special attention to the case where u is close to one. Indeed, the double limit $u \rightarrow 1$ and $Y \rightarrow \infty$ turns out to be quite subtle, and the improper handling of it may be at the origin of the rather curious result reported recently in Ref. [35], namely, the existence of a ‘grey disc’ limit as $Y \rightarrow \infty$. Second, on the basis of the evolution equation for $Z(u; Y)$, Eq. (2.11), we shall deduce a formal correspondence between the toy model considered throughout this paper and the (zero-dimensional) reaction model $A \rightarrow AA$ which has been used in Ref. [35] (see also Appendix A above).

The rather subtle nature of the double limit $u \rightarrow 1$ and $Y \rightarrow \infty$ can be anticipated without doing any calculation, via the following argument: For $u = 1$, we have $Z(u = 1; Y) = \sum_{n=1}^{\infty} P_n(Y) = 1$ for any Y , by probability conservation, whereas for $u < 1$, $Z(u; Y) \rightarrow 0$ when $Y \rightarrow \infty$, as intuitive from the fact that all the probabilities $P_n(Y)$ vanish exponentially in this limit, and it will be explicitly checked below.

The dominant behaviour of $Z(u; Y)$ at high energy depends upon the ratio between u and β , as explained in Sect. 3:

(i) For $\beta < u < 1$, $Z(u; Y)$ is dominated by the typical configurations, distributed according to Eq. (3.31). By using the latter within Eq. (2.9), one easily finds¹⁶

$$\frac{dZ}{dY} = \frac{1-u}{\beta} Z(u) \quad (B.1)$$

which the solution displayed in Eq. (B.2).

$$Z(u; Y) = \exp\left[-\frac{1-u}{\beta}(Y - Y_c)\right] \quad \text{for } Y > Y_c \text{ and } \beta < u < 1: \quad (B.2)$$

The support of this function is strongly peaked near $u = 1$, within a distance $1 - u = (Y - Y_c)/\beta$ which becomes smaller and smaller with increasing energy and/or decreasing β . But if we let $Y \rightarrow \infty$ for fixed $u < 1$ (even arbitrarily close to 1), then $Z(u; Y)$ vanishes exponentially, as anticipated.

(ii) For $u < \beta$, $Z(u; Y)$ is rather controlled by the rare configurations which are dilute, and the corresponding contribution has been already computed in Sect. 3.1. Namely, this is given by Eq. (3.18) in which we replace $m \rightarrow u$:

$$Z(u; Y) \sim \frac{u}{1 - (u = \beta)} e^{-Y} \quad \text{for } Y > Y_c \text{ and } 0 < u < \beta: \quad (B.3)$$

Once again, this vanishes exponentially when $Y \rightarrow \infty$ at fixed (and non-zero) u .

tion in terms of a reaction–diffusion process with ‘BFKL Pomerons’, which appears to be self-dual and thus formally consistent with boost invariance. Note, however, that in that construction, one has given up multiple scattering, that is, one has used a different factorization scheme in which the individual dipoles (from the target and the projectile) are allowed to scatter only once.

¹⁶ The same result can be also obtained from Eq. (2.11), by noticing that, for large Y and u sufficiently close to one, one can simplify that equation by neglecting $Z(u)$ as compared to $Z(u)$.

Following Ref. [17], let us now introduce the following function

$$N(u; Y) = 1 - Z(u; Y); \quad (\text{B.4})$$

which for $u = 1$ yields the scattering amplitude h_{ti} for an external dipole: $N(u = 1; Y) = h_{\text{ti}}$. From the previous discussion it is clear that $N(u; Y) \rightarrow 1$ when $Y \rightarrow 1$ at fixed $u < 1$; this is true, in particular, for $u = 0$, in which case it represents the black disk limit for h_{ti} . On the other hand, $N(u = 1; Y) = 0$ for any Y and, moreover, if Y is large but fixed, then one can always find a value of u sufficiently close to 1 such that $N(u; Y)$ is arbitrarily small.

We are now prepared to appreciate a potential problem with the arguments in Ref. [35]. There, the function $N(u; Y)$ has been somehow abusively interpreted as a ‘scattering amplitude’ for *arbitrary* values of u and Y , i.e., without enforcing the physical requirement that $u = 1$. (In Ref. [35], u is taken to be a fixed parameter, denoted as $1 = u$, and generally chosen as $u = 1.6$.) Then, the high-energy behaviour is investigated by increasing Y and simultaneously decreasing $1 - u$ (i.e., by letting u to approach 1 from the below). Thus, not surprisingly (in view of our previous arguments), the authors of Ref. [35] find that, for u sufficiently close to 1, $N(u; Y)$ remains significantly smaller than one within a large, but *finite*, range of values of Y and, moreover, it drops down to zero when $u \rightarrow 1$. This is the behaviour interpreted by them as a signal of a ‘grey disk limit’ at high energy.

However, the analysis in Ref. [35] does not tell us what happens in the *actual* high-energy limit for the scattering amplitude, which is the limit $Y \rightarrow 1$ for fixed $u = 1$. As for the fact that $N(u; Y) \rightarrow 0$ as $u \rightarrow 1$, this is merely the constraint of probability conservation, as we explained above. In other terms, we suspect that the result in Ref. [35] is just an artifact of improperly taking the high-energy limit.

Strictly speaking, the analysis in Ref. [35] has been performed within the context of a different model — a zero-dimensional reaction model (cf. Appendix A) —, but this difference should not affect our present arguments, since the behaviour of $Z(u; Y)$ in the interesting region is the same in both models. In fact, these two models can be explicitly related, as we explain now: the reaction model of Ref. [35] can be obtained as a ‘weak coupling limit’ of our present model. To see this, let us expand $Z(u) = Z(u) = Z(u) = Z(u)$ in the r.h.s. of Eq. (2.11) to second order in u . This yields the following equation:

$$\frac{dZ}{dY} = u(1 - u) \left(\frac{\partial Z}{\partial u} - \frac{u}{2} \frac{\partial^2 Z}{\partial^2 u} \right); \quad (\text{B.5})$$

This is a partial differential equation of second order in u , similarly to that for the reaction model used in Ref. [35]: the first-order derivative term inside the parentheses describes particles splitting ($A \rightarrow AA$) whereas the second-order derivative term corresponds to particle recombination ($AA \rightarrow A$). The analogy is complete provided one identifies $u = 2$, with the rate for recombination, cf. Eq. (A.5) (which is reasonable since both u and 2 are of order $\frac{2}{s}$ in the correspondence with QCD) and one replaces $u \rightarrow 1$ in the coefficient of the second-order derivative term (which is again reasonable, since recombination is important at large Y , where Z is indeed peaked near $u = 1$, as we have seen).

Note however that the expansion in powers of u leading from Eq. (2.11) to Eq. (B.5) is only formal, as anticipated, since the higher derivatives of Z with respect to u are parametrically large, as obvious from Eq. (B.2) — e.g., $(\partial \ln Z / \partial u) \sim (Y - Y) = \dots$, which invalidates the

expansion.

C A useful sum

In this Appendix we calculate the following sum (with $x = 1$)

$$S_1(x) = \sum_{n=1}^{\infty} \frac{x^n}{1 - x^n}; \quad (C.1)$$

which has appeared to be important at many places of our presentation. Notice that this sum (up to the prefactor) is equal to the double sum $\sum_{m=1}^{\infty} \sum_{n=1}^{\infty} x^{mn}$, which cannot be expressed in terms of known functions. Nevertheless, we can obtain an analytic form for $S_1(x)$, by keeping the first few terms in a series expansion and here we shall work up to order $O(x^2)$. (Of course, the summation can be easily evaluated numerically, since rapidly converging for any $x < 1$.)

One can convert the sum into an integral by making use of the Euler–McLaurin summation formula, which may be written as

$$\sum_{n=1}^{\infty} h_n = \int_1^{\infty} dn h(n) + \frac{1}{2} h(1) + 2 \sum_{k=1}^{\infty} \frac{(-1)^k (2k)!}{(2\pi)^{2k}} h^{(2k-1)}(1); \quad (C.2)$$

With $h(n) = \frac{x^n}{1 - x^n}$, it is straightforward to calculate the integral and we obtain

$$\int_1^{\infty} dn \frac{x^n}{1 - x^n} = \frac{\ln x}{\ln(1 - x)} = \ln \frac{1}{1 - x} = \frac{1}{2} \ln \frac{1}{1 - x} + O(x^2); \quad (C.3)$$

As expected the integral contains the dominant contribution for small x and which is equal to $\ln(1 - x)$. It is trivial to obtain the contribution of the second term in Eq. (C.2) which is

$$\frac{1}{2} h(1) = \frac{1}{2} \ln 2; \quad (C.4)$$

For the contribution of the third term in Eq. (C.2) we need the $(2k - 1)$ -th derivative of $h(n)$ at $n = 1$ which to the order of interest reads

$$h^{(2k-1)}(1) = (-1)^{k-1} (2k - 1)! \frac{1}{2} + O(x^2); \quad (C.5)$$

Notice that now we have to sum a series whose terms are growing factorially, however the terms are alternating sign and the series is Borel summable. Thus we can write the third term as

$$\begin{aligned} \text{third} &= 2 \ln 2 - \frac{1}{2} \sum_{k=1}^{\infty} \frac{(-1)^k (2k)! (2k)}{(2\pi)^{2k}} \\ &= 2 \ln 2 - \frac{1}{2} \int_0^{\infty} \frac{db}{b} e^{-b} \sum_{k=1}^{\infty} \frac{(-1)^k (2k)!}{2} \frac{b^{2k}}{2} \\ &= 1 - \frac{1}{2} \int_0^{\infty} \frac{db}{b} e^{-b} \frac{b}{2} \coth \frac{b}{2} = \frac{1}{2} \ln 2 - \frac{1}{2} \ln 2 = 0; \end{aligned} \quad (C.6)$$

Adding the three contributions obtained in Eqs. (C.3), (C.4) and (C.6) we finally arrive at

$$S_1(\epsilon) = \ln \frac{1}{\epsilon} + \frac{1}{2} \ln \frac{1}{\epsilon} - \frac{1+2\epsilon}{4} + O(\epsilon^2): \quad (C.7)$$

Similarly one can obtain the other sums encountered in Eq. (3.24). One finds

$$S_r(\epsilon) = \sum_{n=1}^{\infty} \frac{1}{(1-\epsilon^n)^r} = \zeta(r) + O(\epsilon) \quad \text{for } r \geq 2: \quad (C.8)$$

References

- [1] A.H. Mueller and G.P. Salam, *Nucl. Phys.* **B475** (1996) 293.
- [2] A.H. Mueller, *Nucl. Phys.* **B415** (1994) 373; A.H. Mueller, B. Patel, *Nucl. Phys.* **B425** (1994) 471.
- [3] A.H. Mueller, *Nucl. Phys.* **B437** (1995) 107.
- [4] G.P. Salam, *Nucl. Phys.* **B449** (1995) 589; *Nucl. Phys.* **B461** (1996) 512.
- [5] I. Balitsky, *Nucl. Phys.* **B463** (1996) 99; *Phys. Lett.* **B518** (2001) 235; “High-energy QCD and Wilson lines”, arXiv:hep-ph/0101042.
- [6] Yu.V. Kovchegov, *Phys. Rev.* **D60** (1999) 034008; *ibid.* **D61** (1999) 074018.
- [7] J. Jalilian-Marian, A. Kovner, A. Leonidov and H. Weigert, *Nucl. Phys.* **B504** (1997) 415; *Phys. Rev.* **D59** (1999) 014014; J. Jalilian-Marian, A. Kovner and H. Weigert, *Phys. Rev.* **D59** (1999) 014015; A. Kovner, J. G. Milhano and H. Weigert, *Phys. Rev.* **D62** (2000) 114005.
- [8] H. Weigert, *Nucl. Phys.* **A703** (2002) 823.
- [9] E. Iancu, A. Leonidov and L. McLerran, *Nucl. Phys.* **A692** (2001) 583; *Phys. Lett.* **B510** (2001) 133; E. Ferreiro, E. Iancu, A. Leonidov and L. McLerran, *Nucl. Phys.* **A703** (2002) 489.
- [10] J.-P. Blaizot, E. Iancu and H. Weigert, *Nucl. Phys.* **A713** (2003) 441.
- [11] E. Iancu and A.H. Mueller, *Nucl. Phys.* **A730** (2004) 460.
- [12] E. Iancu and A.H. Mueller, *Nucl. Phys.* **A730** (2004) 494.
- [13] S. Munier and R. Peschanski, *Phys. Rev. Lett.* **91** (2003) 232001; *Phys. Rev.* **D69** (2004) 034008; *ibid.* **D70** (2004) 077503.
- [14] A.H. Mueller and A.I. Shoshi, *Nucl. Phys.* **B692** (2004) 175.
- [15] E. Iancu, A.H. Mueller and S. Munier, *Phys. Lett.* **B606** (2005) 342.
- [16] E. Levin and M. Lublinsky, *Phys. Lett.* **B607** (2005) 131.
- [17] E. Iancu and D.N. Triantafyllopoulos, *Nucl. Phys.* **A756** (2005) 419.
- [18] E. Iancu and D.N. Triantafyllopoulos, *Phys. Lett.* **B610** (2005) 253.
- [19] A.H. Mueller, A.I. Shoshi, and S.M.H. Wong, *Nucl. Phys.* **B715** (2005) 440.
- [20] E. Levin and M. Lublinsky, *Nucl. Phys.* **A763** (2005) 172.
- [21] A. Kovner and M. Lublinsky, *Phys. Rev.* **D71** (2005) 085004.
- [22] A. Kovner and M. Lublinsky, *Phys. Rev. Lett.* **94** (2005) 181603.
- [23] J.-P. Blaizot, E. Iancu, K. Itakura, and D.N. Triantafyllopoulos, *Phys. Lett.* **B615** (2005) 221.
- [24] Y. Hatta, E. Iancu, L. McLerran, A. Stasto, D.N. Triantafyllopoulos, *Nucl. Phys.* **A764** (2006) 423.

- [25] I. Balitsky, *Phys. Rev.* **D72** (2005) 074027.
- [26] E. Iancu, G. Soyez and D.N. Triantafyllopoulos, *Nucl. Phys.* **A768** (2006) 194.
- [27] C.W. Gardiner, *Handbook of Stochastic Methods*, Springer, Berlin, 2004.
- [28] For a recent review, see W. Van Saarloos, *Phys. Rep.* **386** (2003) 29.
- [29] M. Braun, *Phys. Lett.* **B483** (2000) 115; “Conformal invariant equations for nucleus-nucleus scattering in perturbative QCD with $N_c \rightarrow 1$ ”, arXiv:hep-ph/0504002.
- [30] G. Soyez, *Phys. Rev.* **D72** (2005) 016007.
- [31] R. Enberg, K. Golec-Biernat, and S. Munier, *Phys. Rev.* **D72** (2005) 074021.
- [32] P. Rembiesa and A.M. Stasto, *Nucl. Phys.* **B725** (2005) 251.
- [33] A. Kovner and M. Lublinsky, *Nucl. Phys.* **A767** (2006) 171.
- [34] A. I. Shoshi and B.-W. Xiao, *Phys. Rev.* **D73** (2006) 094014; *Diffraction dissociation including pomeron loops in zero transverse dimensions*, arXiv:hep-ph/0605282.
- [35] M. Kozlov and E. Levin, “Solution for the BFKL Pomeron Calculus in zero transverse dimensions” hep-ph/0604039.
- [36] L. McLerran and R. Venugopalan, *Phys. Rev.* **D49** (1994) 2233; *ibid.* **49** (1994) 3352; *ibid.* **50** (1994) 2225.
- [37] E. Iancu, A. Leonidov and L. McLerran, “The Colour Glass Condensate: An Introduction”, arXiv:hep-ph/0202270. Published in *QCD Perspectives on Hot and Dense Matter*, Eds. J.-P. Blaizot and E. Iancu, NATO Science Series, Kluwer, 2002;
E. Iancu and R. Venugopalan, “The Color Glass Condensate and High Energy Scattering in QCD”, arXiv:hep-ph/0303204. Published in *Quark-Gluon Plasma 3*, Eds. R.C. Hwa and X.-N. Wang, World Scientific, 2003.
- [38] E. Iancu, K. Itakura, and L. McLerran, *Nucl. Phys.* **A708** (2002) 327.
- [39] A.H. Mueller and D.N. Triantafyllopoulos, *Nucl. Phys.* **B640** (2002) 331.
- [40] D.N. Triantafyllopoulos, *Nucl. Phys.* **B648** (2003) 293.
- [41] Y. Hatta, E. Iancu, C. Marquet, G. Soyez, and D.N. Triantafyllopoulos, *Nucl. Phys.* **A773** (2006) 95.
- [42] E. Iancu, C. Marquet, and G. Soyez, “Forward gluon production in hadron-hadron scattering with Pomeron loops”, arXiv:hep-ph/0605174.
- [43] A. H. Mueller, *Nucl. Phys.* **B558** (1999) 285.
- [44] E. Iancu and L. McLerran, *Phys. Lett.* **B510** (2001) 145.
- [45] A. H. Mueller, *Nucl. Phys.* **B643** (2002) 501.
- [46] E. Iancu, K. Itakura, and L. McLerran, *Nucl. Phys.* **A724** (2003) 181.
- [47] L.N. Lipatov, *Sov. J. Nucl. Phys.* **23** (1976) 338;
E.A. Kuraev, L.N. Lipatov and V.S. Fadin, *Zh. Eksp. Teor. Fiz* **72**, 3 (1977) (*Sov. Phys. JETP* **45** (1977) 199); Ya.Ya. Balitsky and L.N. Lipatov, *Sov. J. Nucl. Phys.* **28** (1978) 822.
- [48] I. Balitsky, *Phys. Rev. Lett.* **81** (1998) 2024; *Phys. Rev.* **D60** (1999) 014020.
- [49] C. Marquet, A.H. Mueller, A.I. Shoshi, and S.M.H. Wong *Nucl. Phys.* **A762** (2005) 252.
- [50] Y. Hatta, E. Iancu, L. McLerran, and A. Stasto, *Nucl. Phys.* **A762** (2005) 272.